A joint soil vegetation atmospheric water tagging procedure with WRF Hydro: implementation and application to the case of precipitation partitioning in the Upper Danube River Basin

Joël Arnault, Jianhui Wei, Thomas Rummler, Benjamin Fersch, Zhenyu Zhang, Gerlinde Jung, Sven Wagner, Harald Kunstmann

Angaben zur Veröffentlichung / Publication details:

Arnault, Joël, Jianhui Wei, Thomas Rummler, Benjamin Fersch, Zhenyu Zhang, Gerlinde Jung, Sven Wagner, and Harald Kunstmann. 2019. "A joint soil vegetation atmospheric water tagging procedure with WRF Hydro: implementation and application to the case of precipitation partitioning in the Upper Danube River Basin." *Water Resources Research* 55 (7): 6217–43. https://doi.org/10.1029/2019wr024780.

Water Resources Research

RESEARCH ARTICLE
10.1029/2019WR024780

A Joint Soil-Vegetation-Atmospheric Water Tagging Procedure With WRF-Hydro: Implementation and Application to the Case of Precipitation Partitioning in the Upper Danube River Basin

Joël Arnault[1], Jianhui Wei[1], Thomas Rummler[2], Benjamin Fersch[1], Zhenyu Zhang[1,2], Gerlinde Jung[3], Sven Wagner[2,4], and Harald Kunstmann[1,2]

[1]Institute of Meteorology and Climate Research, Karlsruhe Institute of Technology, Garmisch-Partenkirchen, Germany, [2]Institute of Geography, University of Augsburg, Augsburg, Germany, [3]MARUM, Centre for Marine Environmental Research, University of Bremen, Bremen, Germany, [4]Fraunhofer Institute for Industrial Engineering IAO, Stuttgart, Germany

Key Points:
- A joint soil-vegetation-atmospheric water tagging procedure is incorporated into the WRF and WRF-Hydro models
- Lateral terrestrial water flow slightly modifies the partitioning of precipitation event water among terrestrial-atmospheric compartments
- The procedure can be adapted to track water from any water compartment in WRF-Hydro, which widens the range of future application studies

Correspondence to:
J. Arnault,
joel.arnault@kit.edu

Citation:
Arnault, J., Wei, J., Rummler, T., Fersch, B., Zhang, Z., Jung, G., et al. (2019). A joint soil-vegetation-atmospheric water tagging procedure with WRF-Hydro: Implementation and application to the case of precipitation partitioning in the upper Danube river basin. *Water Resources Research*, *55*, 6217–6243. https://doi.org/10.1029/2019WR024780

Received 16 JAN 2019
Accepted 2 JUL 2019
Accepted article online 8 JUL 2019
Published online 30 JUL 2019

Abstract Atmospheric models such as the Weather Research and Forecasting (WRF) model provide a tool to evaluate the behavior of regional hydrological cycle components, including precipitation, evapotranspiration, soil water storage, and runoff. Recent model developments have focused on coupled atmospheric-hydrological modeling systems, such as WRF-Hydro, in order to account for subsurface, overland, and river flow and potentially improve the representation of land-atmosphere interactions. The aim of this study is to investigate the contribution of lateral terrestrial water flow to the regional hydrological cycle, with the help of a joint soil-vegetation-atmospheric water tagging procedure newly developed in the so-called WRF-tag and WRF-Hydro-tag models. An application of both models for the high precipitation event on 15 August 2008 in the German and Austrian parts of the upper Danube river basin (94,100 km^2) is presented. The precipitation that fell in the basin during this event is considered as a water source, is tagged, and subsequently tracked for a 40-month period until December 2011. At the end of the study period, in both simulations, approximately 57% of the tagged water has run off, while 41% has evaporated back to the atmosphere, including 2% that has recycled in the upper Danube river basin as precipitation. In WRF-Hydro-tag, the surface evaporation of tagged water is slightly enhanced by surface flow infiltration and slightly reduced by subsurface lateral water flow in areas with low topography gradients. This affects the source precipitation recycling only in a negligible amount.

1. Introduction

Global and regional climate models have the ability to predict the atmospheric and terrestrial components of the hydrological cycle, which are atmospheric water, precipitation, soil moisture, evaporation from the Earth surface, and runoff (e.g., Dirmeyer, 2013). These models are routinely used to evaluate the effect of climate and land use change on, for example, precipitation (e.g., Dieng et al., 2017; Im et al., 2014; Laux et al., 2017; Mahmood et al., 2014; Pielke et al., 2011; Quesada et al., 2017; Serdeczny et al., 2016; Smiatek et al., 2016). However, such models generally have a crude representation of terrestrial hydrology and generally neglect the horizontal transport of terrestrial water in dependence of topography and groundwater depth.

The partitioning of precipitation among the terrestrial water components is a complex process quantitatively not fully understood in all its details yet (Brooks et al., 2015). As noted by Seneviratne et al. (2010), land surface model (LSM) improvements are required in order to better represent soil moisture-precipitation interaction and improve the realism of model results, thus making climate models more suitable for water resources research. Potential LSM improvements can be reached by enhancing the description of physical processes (e.g., Niu et al., 2011), as well as by refining the soil feature and land use information (e.g., Gao et al., 2008).

Recent studies showed that considering the horizontal transport of terrestrial water in a climate model has an impact on precipitation (e.g., Arnault, Wagner, et al., 2016; Arnault et al., 2018; Kerandi et al., 2017; Larsen et al., 2016; Maxwell et al., 2007; Rahman et al., 2015; Rummler et al., 2019; Senatore et al., 2015;

Wagner et al., 2016; Zhang et al. 2019). Indeed, spatially redistributing soil moisture modifies surface fluxes, which potentially affects boundary layer dynamics, convection initiation and precipitation (e.g., Pielke, 2001).

The present study aims at further investigating and quantifying the contribution of lateral terrestrial water flow to the regional hydrological cycle by using a climate model which allows considering the horizontal transport of terrestrial water. For this purpose, as in, for example, Senatore et al. (2015), Arnault, Wagner, et al., 2016, Arnault et al., 2018), and Kerandi et al. (2017), we generate and compare two simulations with (1) the Weather Research and Forecasting (WRF) model (Skamarock & Klemp, 2008), a traditional climate model which considers the terrestrial water transport as being only vertical, and (2) the hydrologically enhanced version WRF-Hydro (Gochis et al., 2015) which includes surface and subsurface lateral water flow.

The atmospheric branch of the hydrological cycle simulated by a climate model can be examined with a surface evaporation tagging method, which consists in tracking the evaporated water online, that is throughout the model run, from a source region until it precipitates or is advected outside of the simulation domain (Arnault, Knoche, et al., 2016; Dominguez et al., 2016; Insua-Costa & Miguez-Macho, 2018; Knoche & Kunstmann, 2013; Sodemann et al., 2009; Wei et al., 2015, 2016). It is noted that Arnault, Knoche, et al. (2016) and Dominguez et al. (2016) and Insua-Costa and Miguez-Macho's (2018) tagging methods were independently developed in the WRF model. The surface evaporation tagging method allows to quantify regional precipitation recycling, which is the relative amount of local precipitation originating from local surface evaporation in a region. For a 1×10^6-km^2 area in the West African monsoon region, Arnault, Knoche, et al. (2016) found a regional precipitation recycling of about 12%. A similar number was found by Dominguez et al. (2016) for an approximately 2 times smaller area in the North American monsoon region, as a mountain ridge enhances the recycling of precipitation in this particular region.

The terrestrial branch of the hydrological cycle simulated by a LSM can be examined with a precipitation tagging method, which consists in tracking online the precipitation from a source region until it runs off or evaporates at the surface. Recently, Hu et al. (2018) presented the first implementation of such a precipitation tagging method within the community Noah LSM with multiparameterization options (Noah-MP, Niu et al., 2011). Applying their method to an extreme precipitation event at the beginning of the cold season in the U.S. Pacific Northwest, Hu et al. (2018) found that approximately 30% of the event water remains in the soil after a 6-month period, so that the selected event could contribute to local surface evaporation and groundwater recharge even after a 6-month period. At the watershed scale, Hu et al. (2018) further showed that relaxing the assumption of complete mixing between tagged and total soil moisture shortens the transit time of event water in the first meter of soil, which better fits transit time derived from isotope measurements. For the entire simulation domain covering a land area of 80,000 km^2, however, Hu et al. (2018) could not assess the benefit of relaxing the complete mixing assumption, as observations of transit time at this scale are not available.

The above-cited water tagging methods allow to evaluate only separately the atmospheric and terrestrial branches of the hydrological cycle. Nevertheless, a better understanding of water pathways in the Earth system could be reached by adapting these water tagging methods to both atmospheric and terrestrial water compartments within one model. In this study and for the first time, it is proposed to join the precipitation tagging method (Hu et al., 2018) and surface evaporation tagging method (e.g., Arnault, Knoche, et al., 2016; Insua-Costa & Miguez-Macho, 2018) within the so-called joint soil-vegetation-atmospheric water tagging (SVA-TAG) procedure and apply it for a large river basin and a real event. In particular, we extend Arnault, Knoche, et al. (2016) WRF tagging method to the terrestrial branch of the hydrological cycle within the newly developed WRF-tag and WRF-Hydro-tag models. Similar as in Hu et al. (2018), the SVA-TAG procedure consists in tracking precipitation through the terrestrial water compartments, (1) vertically within the Noah LSM (Chen & Dudhia, 2001) in both WRF-tag and in WRF-Hydro-tag, (2) additionally horizontally within the surface and subsurface routing modules, and (3) through the atmospheric compartment for the evaporated part. In comparison to Hu et al.'s (2018) precipitation tagging method, the one proposed here also includes atmospheric water tracking. In the following sections, with the term "precipitation tagging" we refer to the method including both terrestrial and atmospheric water tracking.

The objective of precipitation tagging with the SVA-TAG procedure is to evaluate the fate of precipitated water in both the soil and in the atmosphere if it evaporates. The contribution of lateral terrestrial water

flow to the regional hydrological cycle is investigated by comparing precipitation tagging results from two simulations performed with WRF-tag and WRF-Hydro-tag.

A detailed description of the SVA-TAG procedure newly developed in WRF-tag and WRF-Hydro-tag is presented in section 2. The setup of an application case study is provided in section 3, and results are discussed in section 4. A summary and perspectives are finally given in section 5.

2. Joint SVA-TAG Procedure and Budget Diagnostics

This section details the implementation of the joint soil-vegetation atmospheric water tagging (SVA-TAG) procedure within the WRF model (Skamarock & Klemp, 2008) and its hydrologically enhanced version WRF-Hydro (Gochis et al., 2015). These two climate models share a common description of the atmospheric physics. The difference between WRF and WRF-Hydro lies in the treatment of terrestrial hydrological processes, as the lateral terrestrial water flow is neglected in WRF, but considered in WRF-Hydro, as illustrated in Figure 1. The WRF and WRF-Hydro models used in this study are based on the WRF version 3.7 (available at http://www2.mmm.ucar.edu/wrf/users/downloads.html). The selected hydrological extension of WRF-Hydro is based on the version 3.0 (available at https://ral.ucar.edu/projects/wrf_hydro/model-code), which is compatible with the WRF model version 3.7.

The SVA-TAG procedure is an online method, which is used to track precipitation, with the objective to more precisely analyze and quantify the water pathways through the terrestrial and atmospheric compartments of the hydrological cycle. The SVA-TAG procedure is developed in the WRF and WRF-Hydro models, by adapting and extending the atmospheric water tagging method already available in the WRF model version 3.5.1 (Arnault, Knoche, et al., 2016). The tagging-enhanced models versions are referred to as WRF-tag and WRF-Hydro-tag.

For the precipitation tracking application, SVA-TAG takes as input the source precipitation P^{source} (m/s), defined for a source region and a time period. The method consists in tagging and tracking this water source through the land surface and through the atmosphere if evaporation occurs. The fate of the tagged soil-vegetation-atmospheric water is described by tagged variables and tagged prognostic equations newly implemented in the source code. In both terrestrial and atmospheric water compartments, the total and tagged water are assumed to be completely mixed, so that the physical processes acting on tagged water are determined with tagged ratio weights, as detailed in the following sections.

2.1. Terrestrial Water Tagging in WRF-tag

In the WRF configuration considered in this study, the surface evaporation is computed with the Noah LSM (Chen & Dudhia, 2001). Noah LSM is a column model, so that only the vertical water flow is taken into account. A one-layer snowpack, a one-layer canopy water, and a multilayer soil moisture are resolved. Four additional prognostic variables are considered to describe the fate of tagged terrestrial water in WRF-tag, which are the tagged snow equivalent water content W_s^{tagged} (m), the tagged canopy water W_c^{tagged} (m), the tagged liquid soil moisture $\theta_{\text{liq}}^{\text{tagged}}$ (−), and the tagged frozen soil moisture $\theta_{\text{ice}}^{\text{tagged}}$ (−). The prognostic equation of W_s^{tagged} is implemented as follows:

$$\underbrace{\left(W_s^{\text{tagged}}\right)_t}_{a1} = \underbrace{P_{\text{solid}}^{\text{source}}}_{a2} - \underbrace{r_s R_{\text{melt}}}_{a3} - \underbrace{r_s E_s}_{a4} \tag{1}$$

The subscript t (s) stands for the time derivate, and $\left(W_s^{\text{tagged}}\right)_t$ (m/s) is referred to as the tendency of W_s^{tagged}. $P_{\text{solid}}^{\text{source}}$ (m/s) is the solid part of the source precipitation, R_{melt} (m/s) is the total snowmelt, E_s (m/s) is the total snow sublimation, and r_s (−) is the ratio between tagged and total snow equivalent water content. In equation (1), the tendency of W_s^{tagged} ($a1$) is the sum of the following source and sink terms: source snowfall ($a2$), tagged snowmelt ($a3$), and tagged snow sublimation ($a4$). A list of symbols and mathematical operators is provided in the Appendix A.

The prognostic equation of W_c^{tagged} is implemented as follows:

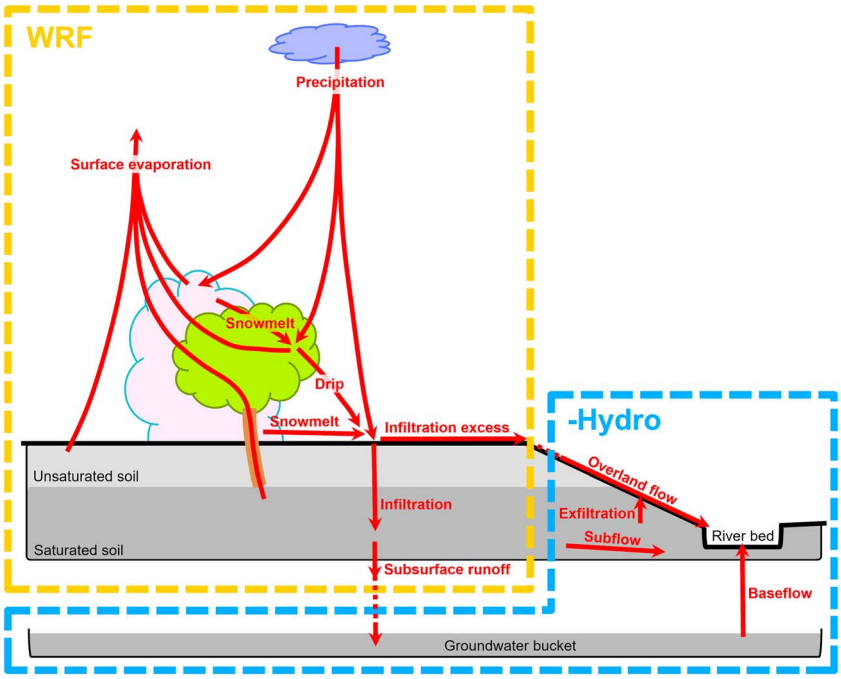

Figure 1. Conceptual view of the terrestrial compartments in the WRF and WRF-Hydro modeling systems detailed in section 2. Water fluxes are represented by red arrows. WRF = Weather Research and Forecasting.

$$\underbrace{\left(W_c^{\text{tagged}}\right)_t}_{b1} = \underbrace{\sigma_f P_{\text{liq}}^{\text{source}}}_{b2} + \underbrace{\sigma_f r_s R_{\text{melt}}}_{b3} - \underbrace{r_c R_{\text{drip}}}_{b4} - \underbrace{r_c E_c}_{b5} \tag{2}$$

σ_f (−) is the vegetation fraction, $P_{\text{liq}}^{\text{source}}$ (m/s) is the liquid part of the source precipitation, R_{drip} (m/s) is the total water dripping from the canopy to the bare soil, E_c (m/s) is the total canopy water evaporation, and r_c (−) is the ratio between tagged and total canopy water. Dripping occurs when the amount of canopy water exceeds a threshold. In equation (2), the tendency of W_c^{tagged} ($b1$) is the sum of the following source and sink terms: source rainfall falling on the canopy ($b2$), tagged snowmelt on the canopy ($b3$), tagged canopy water drip ($b4$), and tagged canopy water evaporation ($b5$). In this approach, the canopy interception of solid source precipitation is not explicitly represented.

The tagged water falling on bare soil is referred to as $P_{\text{bare}}^{\text{tagged}}$ (m/s):

$$P_{\text{bare}}^{\text{tagged}} = \left(1-\sigma_f\right)P_{\text{liq}}^{\text{source}} + \left(1-\sigma_f\right)r_s R_{\text{melt}} + r_c R_{\text{drip}} \tag{3}$$

$P_{\text{bare}}^{\text{tagged}}$ is the sum of liquid source precipitation falling on bare soil, tagged snowmelt on bare soil, and tagged canopy water drip. The ratio between $P_{\text{bare}}^{\text{tagged}}$ and the total water falling on bare soil P_{bare} (m/s), as well as the surface infiltration I (m/s), are used to derive the tagged surface infiltration I^{tagged} (m/s):

$$I^{\text{tagged}} = \frac{P_{\text{bare}}^{\text{tagged}}}{P_{\text{bare}}} I \tag{4}$$

Defining the tagged surface runoff R_S^{tagged} (m/s) as the tagged surface infiltration excess, it becomes:

$$R_S^{\text{tagged}} = P_{\text{bare}}^{\text{tagged}} - I^{\text{tagged}} \tag{5}$$

Within each soil layer, the partitioning between $\theta_{\mathrm{liq}}^{\mathrm{tagged}}$ and $\theta_{\mathrm{ice}}^{\mathrm{tagged}}$ is evaluated with a soil freezing/thawing module as follows:

$$\begin{aligned}\left(\theta_{\mathrm{ice}}^{\mathrm{tagged}}\right)_t^{\mathrm{freez/thaw}} &= r_{\theta_{\mathrm{liq}}}\theta_{\mathrm{freezing}} - r_{\theta_{\mathrm{ice}}}\theta_{\mathrm{thawing}} \\ \left(\theta_{\mathrm{liq}}^{\mathrm{tagged}}\right)_t^{\mathrm{freez/thaw}} &= -r_{\theta_{\mathrm{liq}}}\theta_{\mathrm{freezing}} + r_{\theta_{\mathrm{ice}}}\theta_{\mathrm{thawing}}\end{aligned} \tag{6}$$

$\theta_{\mathrm{freezing}}$ (s^{-1}) gives the rate of freezing of the total liquid soil moisture and $\theta_{\mathrm{thawing}}$ (s^{-1}) gives the rate of thawing of the total frozen soil moisture. $r_{\theta_{\mathrm{liq}}}$ (−) is the ratio between tagged and total liquid soil moisture, and $r_{\theta_{\mathrm{ice}}}$ (−) is the ratio between tagged and total frozen soil moisture. $\left(\theta_{\mathrm{ice}}^{\mathrm{tagged}}\right)_t^{\mathrm{freez/thaw}}$ (s^{-1}) and $\left(\theta_{\mathrm{liq}}^{\mathrm{tagged}}\right)_t^{\mathrm{freez/thaw}}$ (s^{-1}) give the rate of change of $\theta_{\mathrm{ice}}^{\mathrm{tagged}}$ and $\theta_{\mathrm{liq}}^{\mathrm{tagged}}$ through freezing/thawing. Tagged frozen soil moisture is considered to be motionless.

Concerning the vertical transport of $\theta_{\mathrm{liq}}^{\mathrm{tagged}}$ in the model soil layers, as already mentioned above, we assume a complete mixing between tagged and total liquid soil moisture (similar to Hu et al., 2018). The prognostic equation of $\theta_{\mathrm{liq}}^{\mathrm{tagged}}$ is derived from the one-dimensional diffusive form of Richard's equation used to describe the vertical transport of the total liquid soil moisture θ_{liq} (−):

$$\underbrace{\Delta z_s\left(\theta_{\mathrm{liq}}^{\mathrm{tagged}}\right)_t}_{c1} = \underbrace{\Delta z_s\left(r_{\theta_{\mathrm{liq}}}D_\theta\left(\theta_{\mathrm{liq}}\right)_z\right)_z}_{c2} + \underbrace{\Delta z_s\left(r_{\theta_{\mathrm{liq}}}K_\theta\right)_z}_{c3} + \underbrace{F_\theta^{\mathrm{tagged}}}_{c4} \tag{7}$$

Subscript z (m) stands for the derivate operator in the vertical direction; Δz_s (m) is the soil layer thickness; D_θ (m^2/s) is the soil water diffusivity; K_θ (m/s) is the hydraulic conductivity; $F_\theta^{\mathrm{tagged}}$ (m/s) represents the tagged external forcing, which is the sum of tagged surface infiltration and tagged direct evaporation E_d^{tagged} (m/s) for the first soil layer and tagged plant transpiration E_t^{tagged} (m/s) for the soil layers within the root depth. E_d^{tagged} and E_t^{tagged} are assumed to be proportional to the relative amount of tagged liquid soil moisture, so that they are computed as the product between total direct evaporation/total transpiration and $r_{\theta_{\mathrm{liq}}}$.

In equation (7), the tendency of tagged liquid soil moisture content ($c1$) is the sum of tagged diffusion ($c2$), tagged conduction ($c3$), and the tagged forcing term ($c4$), in each soil layer. The tagged diffusion and tagged conduction give the amount of tagged liquid soil moisture exchanged between two adjacent soil layers. Following Hu et al. (2018), the tagged diffusion ($c2$) is defined as the total diffusion weighted by $r_{\theta_{\mathrm{liq}}}$ in the soil layer from which θ_{liq} is exchanged through diffusion, which depends on the sign of the vertical gradient of θ_{liq}. Similarly, the tagged conduction ($c3$) is also defined as the total conduction weighted by $r_{\theta_{\mathrm{liq}}}$ in the soil layer from which θ_{liq} is exchanged through conduction. It is emphasized that the soil layer from which θ_{liq} is exchanged through conduction does not vary with the sign of the vertical gradient of θ_{liq}, as conduction of water in the soil is a downward flux. For this reason, contrarily to Hu et al. (2018), the tagged diffusion and tagged conduction in equation (7) are treated separately. The tagged water flux crossing the lower boundary of the bottom soil layer through conduction, which is part of the term ($c3$) in equation (7), is considered as the tagged underground runoff R_G^{tagged} (m/s).

Concerning the implementation of equation (7), as noted by Hu et al. (2018), the total diffusion is not explicitly given by the time-implicit scheme used to solve the Richard's equation in the Noah LSM. Accordingly, this total diffusion is diagnosed in order to calculate the term ($c2$) in equation (7).

The sum of tagged snow sublimation, tagged canopy water evaporation, tagged direct evaporation, and tagged plant transpiration is referred to as the tagged surface evaporation E^{tagged} (m/s). Considering the amount of tagged snow equivalent water, tagged canopy water and tagged soil moisture as the components of the tagged terrestrial water storage S^{tagged} (m), the following budget equation of S^{tagged} can be derived from equations (1)–(7):

$$\underbrace{\left(S^{\text{tagged}}\right)_t}_{d1} = \underbrace{P^{\text{source}}}_{d2} - \underbrace{E^{\text{tagged}}}_{d3} - \underbrace{R_S^{\text{tagged}}}_{d4} - \underbrace{R_G^{\text{tagged}}}_{d5} \tag{8}$$

In equation (8), the tendency of S^{tagged} ($d1$) is the sum of the following source and sink terms: source precipitation ($d2$), tagged surface evaporation ($d3$), tagged surface runoff ($d4$), and tagged underground runoff ($d5$). The terms of equation (8) are added to the WRF model outputs. This equation allows quantifying the partitioning of P^{source} among the terrestrial water compartments.

2.2. Terrestrial Water Tagging in WRF-Hydro-tag

In the WRF-Hydro configuration considered in this study, the Noah LSM is also used to resolve snowpack, canopy water, and soil moisture. In comparison to WRF, WRF-Hydro further resolves surface and subsurface lateral water flow as illustrated in Figure 1. Accordingly, the ponded water W_p (m) is introduced in order to describe overland flow. Furthermore, WRF-Hydro requires a subgrid at higher resolution in order to resolve smaller orographic features for the surface and subsurface routing. The fate of tagged overland flow in WRF-Hydro-tag is evaluated with one additional prognostic variable, which is the tagged ponded water W_p^{tagged} (m). The tagged surface runoff in equation (5) is a source of W_p^{tagged}, so that in WRF-Hydro-tag equation (5) is modified as follows:

$$\left\{\Delta W_p^{\text{tagged}}\right\}_I = \left(P_{\text{bare}}^{\text{tagged}} - I^{\text{tagged}}\right)\Delta_t \tag{9}$$

$\left\{\Delta W_p^{\text{tagged}}\right\}_I$ (m) is the change of W_p^{tagged} due to tagged infiltration excess within a time step Δ_t (s).

W_p^{tagged} and $\theta_{\text{liq}}^{\text{tagged}}$ are conservatively disaggregated on the subgrid at higher horizontal resolution, in order to compute the tagged surface and tagged subsurface routing (described later). The disaggregated tagged ponded water and tagged liquid soil moisture are named $W_p^{\text{hires,tagged}}$ (m) and $\theta_{\text{liq}}^{\text{hires,tagged}}$ (−); the superscript hires indicates that the variable is defined on the subgrid. The disaggregation factor of W_p^{tagged} is determined according to the spatial distribution of the disaggregated total ponded water W_p^{hires} (m), as the ratio between W_p^{hires} and W_p. This disaggregation factor is initialized to 1 and is updated at each time step. Similarly, the disaggregation factor of $\theta_{\text{liq}}^{\text{tagged}}$ is also determined as the ratio between the disaggregated total liquid soil moisture $\theta_{\text{liq}}^{\text{hires}}$ (−) and θ_{liq}.

In WRF-Hydro, exfiltration occurs when, as a result of the disaggregation, $\theta_{\text{liq}}^{\text{hires}}$ becomes larger than the saturated liquid soil moisture. In this case the water excess from the bottom soil layer is exfiltrated upward, till the surface. In WRF-Hydro-tag, tagged exfiltration from a soil layer to the above one, or to the surface, is assumed to be equal to the exfiltration of $\theta_{\text{liq}}^{\text{hires}}$ weighted by the relative amount of $\theta_{\text{liq}}^{\text{hires,tagged}}$ in the considered layer. The change in $W_p^{\text{hires,tagged}}$ associated with this exfiltration process, within a time step, is called $\left\{\Delta W_p^{\text{hires,tagged}}\right\}_E$ (m).

Concerning the subsurface routing module in WRF-Hydro, the available water is defined as the amount of $\theta_{\text{liq}}^{\text{hires}}$ above the field capacity. This available water is determined for each soil column; it is considered as "free" and flows laterally along the water table gradient following the Dupuit-Forcheimer saturated flow assumptions. Each soil column receives available water flow from upstream and provides available water flow toward downstream. The net available water flow is referred to as the net subsurface lateral water flow. In WRF-Hydro-tag, the net tagged subsurface lateral water flow $q_{\text{sub}}^{\text{hires,tagged}}$ (m) is assumed to be the net difference between upstream and downstream tagged available water flow, and is computed as follows:

$$q_{\text{sub}}^{\text{hires,tagged}} = \underbrace{\left\{r_{\text{Cavail}}^{\text{hires}}\right\}^{\text{upstream}}\left\{q_{\text{sub}}^{\text{hires}}\right\}^{\text{IN}}}_{\left\{q_{\text{sub}}^{\text{hires,tagged}}\right\}^{\text{IN}}} - \underbrace{\left\{r_{\text{Cavail}}^{\text{hires}}\right\}^{\text{local}}\left\{q_{\text{sub}}^{\text{hires}}\right\}^{\text{OUT}}}_{\left\{q_{\text{sub}}^{\text{hires,tagged}}\right\}^{\text{OUT}}} \tag{10}$$

$\left\{q_{\text{sub}}^{\text{hires}}\right\}^{\text{IN}}$ (m) is the incoming total available water flow from upstream and $\left\{q_{\text{sub}}^{\text{hires}}\right\}^{\text{OUT}}$ (m) is the outgoing total available water flow toward downstream, following the steepest descent. $r_{C\text{avail}}^{\text{hires}}$ (−) is the ratio between tagged and total available water. The superscript upstream indicates that the ratio is evaluated for the upstream soil column, and the superscript local indicates that the ratio is evaluated for the local soil column. $\left\{q_{\text{sub}}^{\text{hires,tagged}}\right\}^{\text{IN}}$ (m) is the incoming tagged available water flow from upstream, and $\left\{q_{\text{sub}}^{\text{hires,tagged}}\right\}^{\text{OUT}}$ (m) is the outgoing tagged available water flow toward downstream.

Once $q_{\text{sub}}^{\text{hires,tagged}}$ is computed for each soil column, it is vertically distributed as follows. If $q_{\text{sub}}^{\text{hires,tagged}}$ is negative, which means that the soil column loses tagged water, the tagged water amount to be retrieved is removed from the top soil layer downward. If $q_{\text{sub}}^{\text{hires,tagged}}$ is positive, which means that the soil column receives tagged water, the tagged water amount to be added is distributed from the bottom soil layer toward the surface, using the relative amount of tagged liquid soil moisture as a depth-weighting factor. This depth-weighting factor is applied in order to prevent tagged liquid soil moisture in the first soil layer to be directly moved to the bottom soil layer when the tagged liquid soil moisture has not infiltrated to that bottom layer yet. The change in $W_p^{\text{hires,tagged}}$ associated with this subsurface routing process, within a time step, is the tagged exfiltrating subsurface water flow $\left\{\Delta W_p^{\text{hires,tagged}}\right\}_{\text{SSR}}$ (m).

In WRF-Hydro, the subgrid also provides a river channel network, in order to compute the channel flow routing for resolving river discharge. If W_p^{hires} is located on a river channel grid cell, the amount of W_p^{hires} exceeding the retention depth is removed from the land surface and added to the channel river flow. The retention depth is defined as a linear decreasing function of terrain slope, with a default value of 0.001 mm for flat terrain. The change in W_p^{hires} caused by river runoff, within a time step, is called $\left\{\Delta W_p^{\text{hires}}\right\}_{\text{CR}}$ (m). In WRF-Hydro-tag, the change in tagged ponded water caused by river runoff is called $\left\{\Delta W_p^{\text{hires,tagged}}\right\}_{\text{CR}}$ (m) and is computed by using the ratio r_p^{hires} (−) between tagged and total ponded water as weighting factor.

$$\left\{\Delta W_p^{\text{hires,tagged}}\right\}_{\text{CR}} = \left\{r_p^{\text{hires}}\right\}^{\text{local}} \left\{\Delta W_p^{\text{hires}}\right\}_{CR} \tag{11}$$

Concerning the channel flow routing module in WRF-Hydro, water flow in the river channel network is described with a diffusive wave formulation allowing for backwater effects, and channel geometrical parameters and Manning's roughness coefficient prescribed as functions of Strahler stream order (Strahler, 1957). Channel-land surface interaction is, however, not considered in this version of WRF-Hydro, so that the channel flow routing does affect neither W_p^{hires} nor $\theta_{\text{liq}}^{\text{hires}}$. A groundwater bucket can also be activated in order to estimate the baseflow contribution to the channel flow. In the pass-through option, this bucket model collects the underground runoff from the Noah LSM and distributes it to all the channel grid cells of the basin. In this conceptual approach, however, the baseflow does not interact with the land surface. Neither channel flow tagging nor baseflow tagging is included in WRF-Hydro-tag.

Concerning the overland routing module in WRF-Hydro, the lateral flow of W_p^{hires} is computed along the gradient of ponded water elevation using a diffusive wave equation adapted from Julien et al. (1995). Each grid point receives surface water flow from upstream and provides surface water flow toward downstream, which results in a net surface lateral water flow. In WRF-Hydro-tag, the net tagged surface lateral water flow $q_{\text{sfc}}^{\text{hires,tagged}}$ (m) is assumed to be the net difference between upstream and downstream tagged surface water flow, and is computed as follows:

$$q_{\text{sfc}}^{\text{hires,tagged}} = \underbrace{\left\{r_p^{\text{hires}}\right\}^{\text{upstream}} \left\{q_{\text{sfc}}^{\text{hires}}\right\}^{IN}}_{\left\{q_{\text{sfc}}^{\text{hires,tagged}}\right\}^{\text{IN}}} - \underbrace{\left\{r_p^{\text{hires}}\right\}^{\text{local}} \left\{q_{\text{sfc}}^{\text{hires}}\right\}^{\text{OUT}}}_{\left\{q_{\text{sfc}}^{\text{hires,tagged}}\right\}^{\text{OUT}}} \tag{12}$$

$\left\{q_{\text{sfc}}^{\text{hires}}\right\}^{\text{IN}}$ (m) is the incoming total surface flow from the upstream grid point and $\left\{q_{\text{sfc}}^{\text{hires}}\right\}^{\text{OUT}}$ (m) is the outgoing total surface flow toward the downstream grid point, following the steepest descent. Similarly, $\left\{q_{\text{sfc}}^{\text{hires,tagged}}\right\}^{\text{IN}}$ (m) is the incoming tagged surface flow from the upstream grid point and $\left\{q_{\text{sfc}}^{\text{hires,tagged}}\right\}^{\text{OUT}}$ (m) is the outgoing tagged surface flow toward the downstream grid point. The change in tagged ponded water caused by overland flow is called $\left\{\Delta W_p^{\text{hires,tagged}}\right\}_{\text{OVR}}$ (m) and is equal to $q_{\text{sfc}}^{\text{hires,tagged}}$.

In WRF-Hydro-tag, the definition of the tagged surface runoff R_S^{tagged} (m/s) is extended and includes tagged overland flow.

$$R_S^{\text{tagged}} = \frac{\left\{\Delta W_p^{\text{hires,tagged}}\right\}_{\text{CR}}^{\text{agg}} - \left\{\Delta W_p^{\text{hires,tagged}}\right\}_{\text{OVR}}^{\text{agg}}}{\Delta_t} \tag{13}$$

The superscript agg indicates aggregated fields from the finer subgrid to the coarser WRF grid. With this definition, tagged surface runoff is (1) enhanced when tagged ponded water enters a channel grid cell, (2) enhanced when the net tagged overland flow is negative, and (3) reduced when the net tagged overland flow is positive. In WRF-Hydro-tag, the definition of the tagged underground runoff R_G^{tagged} (m/s) is also extended and includes tagged subsurface lateral water flow.

$$\left(R_G^{\text{tagged}}\right)_{\text{WRF-Hydro-tag}} = \left(R_G^{\text{tagged}}\right)_{\text{WRF-tag}} - \frac{\left\{q_{\text{sub}}^{\text{hires,tagged}}\right\}^{\text{agg}}}{\Delta_t} \tag{14}$$

$\left(R_G^{\text{tagged}}\right)_{\text{WRF-tag}}$ is the R_G^{tagged} formulation considered in WRF-tag, and $\left(R_G^{\text{tagged}}\right)_{\text{WRF-Hydro-tag}}$ is the updated R_G^{tagged} formulation considered in WRF-Hydro-tag. With this definition, tagged underground runoff is (1) enhanced when the tagged soil moisture flux crosses the lower boundary of the bottom soil layer through conduction, (2) enhanced when the net tagged subsurface lateral water flow is negative, and (3) reduced when the net tagged subsurface lateral water flow is positive. The advantage of equations (13) and (14) is to allow closing the tagged terrestrial water budget with WRF-Hydro-tag using the same tagged water flux variables as with WRF-tag.

$W_p^{\text{hires,tagged}}$ and $\theta_{\text{liq}}^{\text{hires,tagged}}$ are aggregated back to the coarser WRF grid using a simple mean operator, in order to update W_p^{tagged} and $\theta_{\text{liq}}^{\text{tagged}}$. The prognostic equation of W_p^{tagged} that has been implemented in WRF-Hydro-tag can be written as follows:

$$\underbrace{\left(W_p^{\text{tagged}}\right)_t}_{e1} = \underbrace{\frac{\left\{\Delta W_p^{\text{tagged}}\right\}_I}{\Delta_t}}_{e2} + \underbrace{\frac{\left\{\Delta W_p^{\text{hires,tagged}}\right\}_E^{\text{agg}}}{\Delta_t}}_{e3} + \underbrace{\frac{\left\{\Delta W_p^{\text{hires,tagged}}\right\}_{\text{SSR}}^{\text{agg}}}{\Delta_t}}_{e4} - \underbrace{R_S^{\text{tagged}}}_{e5} \tag{15}$$

In equation (15), the tendency of tagged surface water W_p^{tagged} ($e1$) is the sum of the following source and sink terms: tagged infiltration excess ($e2$), tagged exfiltration ($e3$), tagged exfiltrating subsurface flow ($e4$), and tagged surface runoff ($e5$).

Accordingly, the prognostic equation of tagged column soil moisture content W_θ^{tagged} (m) in WRF-Hydro-tag can be written as follows:

$$\underbrace{\left(W_\theta^{\text{tagged}}\right)_t}_{f1} = \underbrace{I^{\text{tagged}}}_{f2} - \underbrace{E_d^{\text{tagged}}}_{f3} - \underbrace{E_t^{\text{tagged}}}_{f4} - \underbrace{\frac{\left\{\Delta W_p^{\text{hires,tagged}}\right\}_E^{\text{agg}}}{\Delta_t}}_{f5} - \underbrace{\frac{\left\{\Delta W_p^{\text{hires,tagged}}\right\}_{\text{SSR}}^{\text{agg}}}{\Delta_t}}_{f6} - \underbrace{R_G^{\text{tagged}}}_{f7} \tag{16}$$

In equation (16), the tendency of $W_{\theta}^{\text{tagged}}$ ($f1$) is the sum of the following source and sink terms: tagged infiltration ($f2$), tagged direct evaporation ($f3$), tagged plant transpiration ($f4$), tagged exfiltration ($f5$), tagged exfiltrating subsurface flow ($f6$), and tagged underground runoff ($f7$).

The budget of tagged terrestrial water equation (8) implemented in the Noah LSM (section 2.1) can also be used in the WRF-Hydro-tag framework after adding W_{p}^{tagged} to the tagged soil storage variable S^{tagged}. The updated formulations of S^{tagged}, R_{S}^{tagged}, and R_{G}^{tagged} are added to the WRF-Hydro-tag outputs, so that the tagged terrestrial water budgets from WRF-tag and WRF-Hydro-tag simulations can be easily compared. Such a comparison aims at quantifying the effect of lateral terrestrial water flow on the partitioning of P^{source}.

2.3. Atmospheric Water Tagging in WRF-tag and WRF-Hydro-tag

The atmospheric core of the WRF and WRF-Hydro models offers a set of physical parameterizations in order to account for subgrid-scale processes. Subscale atmospheric processes that are usually parameterized are the short and long wave radiation, atmospheric turbulence, and cumulus convection. At moist convection permitting resolution (horizontal grid spacing of the order of a few kilometers) cloud physics can be assumed to be resolved by the microphysics scheme without the help of a cumulus parameterization.

Following Arnault, Knoche, et al. (2016), in case of disabled cumulus parameterization, the tagged surface evaporation E^{tagged} can be tracked in the atmosphere until it precipitates or is advected outside of the simulation domain. This method can be used with both WRF-tag and WRF-Hydro-tag, as these two models share the same atmospheric core. The evaporation tagging method was first implemented within the WRF single-moment five-class microphysics scheme (WSM5) of Hong et al. (2004), and the Yonsei University (YSU) planetary boundary layer (PBL) scheme of Hong et al. (2006). Now, the method is extended and additionally implemented in the WRF single-moment six-class microphysics scheme (WSM6) of Hong and Lim (2006) and the asymetric convective model version 2 (ACM2) PBL scheme of Pleim (2007), in order to widen the range of possible applications. Implementation details are similar to those already provided in Arnault, Knoche, et al. (2016) and are not repeated here for the sake of brevity.

As in Arnault, Knoche, et al. (2016), the tendency equations of tagged water species are vertically and temporally integrated and summed online during the model run, in order to provide the budget equation of the two-dimensional tagged atmospheric water content W^{tagged} (m) in the model outputs:

$$\underbrace{\left(W^{\text{tagged}}\right)_{t}}_{g1} = \underbrace{E^{\text{tagged}}}_{g2} - \underbrace{O_{\text{NET}}^{\text{tagged}}}_{g3} - \underbrace{P^{\text{tagged}}}_{g4} \tag{17}$$

In equation (17), the tendency of W^{tagged} ($g1$) is the sum of the following source and sink terms: tagged surface evaporation ($g2$), net outflow of tagged atmospheric water ($g3$), and tagged precipitation ($g4$). In this approach, P^{tagged} is not further tracked in the soil, except if it falls in the source region during the tagging period, as in this case it is part of P^{source}. Integrating equation (17) spatially in the source region and temporally for a sufficiently long period, the ratio between P^{tagged} and P^{source} gives an estimate of the recycling of the source precipitation occurring in the source region. It is emphasized that the source precipitation recycling aims at quantifying the fate of precipitated water in the atmosphere, whereas the regional precipitation recycling (e.g., Arnault, Knoche, et al., 2016; Dominguez et al., 2016) aims at quantifying the source of a precipitated water, particularly from local surface evaporation in a given region. Therefore, source precipitation recycling and regional precipitation recycling are two distinct measures, and source precipitation recycling results obtained in this study are not directly comparable to regional precipitation recycling results previously published.

The terms of equation (17) are added to the model outputs. This equation allows further on to quantify the partitioning of P^{source} among the atmospheric water compartments in WRF-tag/WRF-Hydro-tag.

3. Application Study

3.1. WRF and WRF-Hydro Models Setup

In order to demonstrate the newly developed SVA-TAG procedure described in section 2, an application of WRF and WRF-Hydro for the upper Danube river basin of Germany and Austria (94,100 km^2, displayed in

Figure 2b) is presented. The study period is 2008–2011, during which Danube streamflow data are available at the location of Kienstock (Austria), the outlet of the subcatchment considered in this study. The choice of this study region is motivated by the fact that this is one of the main river basins in central Europe and the proven reasonable WRF-Hydro performance in this case (Arnault et al., 2018). In the following, the study region is referred to as Δ. Two subregions are also considered, namely, the northern subregion Δ_1 characterized by moderate topography and the southern subregion Δ_2 characterized by steep topography, in order to analyze the respective effects of lateral terrestrial water flow and topography on water pathways.

For the WRF setup, the single domain shown in Figure 2a is considered. It covers the study region Δ, with 150×200 horizontal grid points and a grid spacing of 5 km. With such a horizontal resolution the simulation can be considered as convection-permitting (Karki et al., 2017), so that cumulus parameterization is disabled in this setup. The vertical grid has 50 vertical levels up to 10 hPa. The model is initialized at 0000 UTC on 1 January 2007 and run for five consecutive years, using the 6-hourly operational analyses from the European Center for Medium-range Weather Forecast at 0.125° horizontal resolution for the initial and lateral boundary condition. The model time step is set to 30 s. Following Rummler et al. (2019), the first simulation year is considered as spin-up period for land surface variables. For the parameterization of subgrid-scale processes, the long and short wave radiation schemes of Mlawer et al. (1997) and Dudhia (1989), and the ACM2 PBL schemes are enabled. Microphysical processes are described with the WSM6 scheme and soil processes with the Noah LSM. Using the precipitation data set from the European Climate Assessment & Dataset project (Haylock et al., 2008), Arnault et al. (2018) showed that these WRF parameterization options reduce the precipitation bias for central Europe and are hence suitable for an application in the area of interest.

In the default Noah LSM there are four soil layers with respective thicknesses of 0.1, 0.3, 0.6, and 1.0 m, resulting in a total soil thickness of 2 m. For a precipitation tagging application, as shown by Hu et al. (2018), this vertical gridding is too coarse to fully capture the lag of tagged soil moisture response in deeper layers. Therefore, the default four soil layers are replaced by 20 soil layers with a constant thickness of 0.1 m, thus keeping the total soil thickness of 2 m. The soil layer numbers defining the depths of the root zone, which are provided for each vegetation class in a look-up table, have been modified in order to keep the same root depths as in the default Noah LSM. In comparison to Arnault et al. (2018), the Noah LSM has been calibrated in order to reduce the simulated surface evaporation amounts and improve the resemblance to the surface evaporation product from the model tree ensemble (Jung et al., 2009, 2010). In particular, the bare soil evaporation parameter which has a default value of 2 (see details in Ek et al., 2003) has been set to 4, and the minimum stomatal resistance of the forest land use/land cover classes has been multiplied by a factor of 2.

A WRF-Hydro simulation is also conducted, using the same setup as described above for the *WRF* part. For the *Hydro* part, a subgrid with a grid spacing of 500 m is considered in order to compute subsurface, overland and channel flow routing (Figure 2b). The routing processes are computed with a time step of 30 s, as for the *WRF* part. The subgrid is obtained with the WRF-Hydro Pre-processing Tool. The digital elevation data from the hydrological data and maps based on Shuttle Elevation Derivatives at Multiple Scales (HydroSHEDS) data base (Lehner et al., 2008) serves as input, and the minimal number of pixels to define a stream is set to 3. A groundwater bucket using the pass-through option is also activated, in order to estimate the baseflow contribution in the upper Danube river basin. In this WRF-Hydro setting the default values for surface roughness, lateral hydraulic conductivity, retention depth, and channel parameters are used, except for the Manning coefficients, which have been decreased for calibration purpose, ranging from 0.08 at the stream order 1 to 0.01 at the stream order 8.

WRF and WRF-Hydro model outputs are saved at an hourly interval. In WRF-Hydro, additionally, streamflow is accumulated during the run and saved at a daily interval.

3.2. Model Evaluation

Model results are evaluated with the daily gridded precipitation product from the European Climate Assessment & Dataset project (Haylock et al., 2008), referred to as P_{OBS}, the monthly gridded surface evaporation product from the model tree ensemble (Jung et al., 2009, 2010), referred to as E_{OBS}, and the daily discharge at gauge Kienstock from the Global Runoff Data Center (2015), referred to as Q_{OBS}.

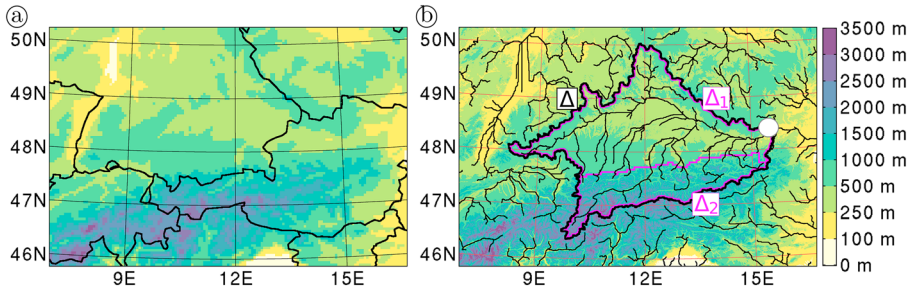

Figure 2. (a) Terrain elevation (meters above sea level) of the 5-km resolution Weather Research and Forecasting domain. The solid black lines delineate the political boundaries. (b) Terrain elevation of the routing grid at 500-m resolution coupled with the Weather Research and Forecasting domain in the WRF-Hydro setup. The thin black lines show river channels with a Strahler stream order equal to or above 5. The bold black contour delineates the part of the upper Danube river basin referred as the study region Δ. Δ is divided into two subregions delineated by the bold magenta contour: Δ_1 characterized by moderate topography in the north, and Δ_2 characterized by steep topography in the south. The white circle indicates the location of the river gauge at Kienstock (Austria). The terrain height scale is given by the colored bar to the right.

Monthly time series of Δ-averaged *P* and *E*, and *Q* at Kienstock are displayed in Figure 3. In WRF, the discharge at Kienstock is evaluated with the Δ-averaged runoff *R*, which is the sum of surface and underground runoff. Both WRF and WRF-Hydro approximately reproduce the observed monthly variations of these three components of the hydrological cycle. Precipitation is mostly overestimated, with an annual difference to observation of +45.5 mm/year (+4.6%) for WRF and 46.8 mm/year (+4.8%) for WRF-Hydro.

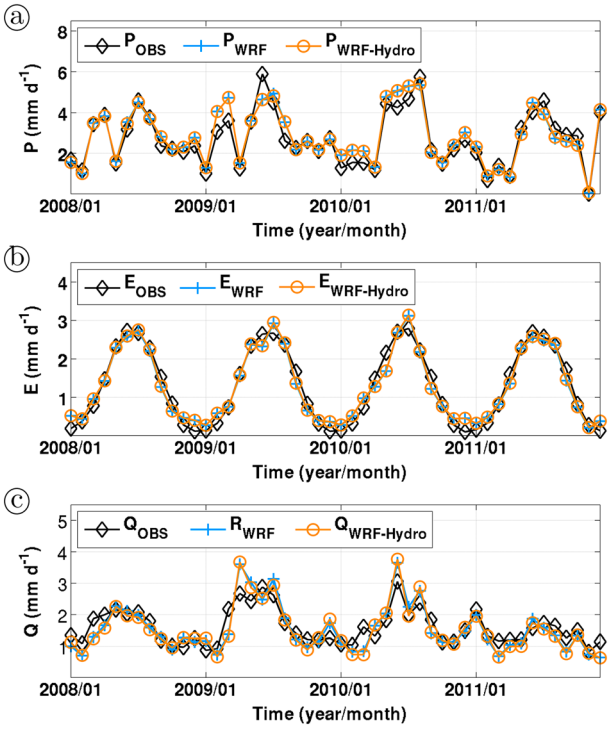

Figure 3. (a) Monthly time series of precipitation *P* (mm/day) from the observational data set, WRF and WRF-Hydro, spatially averaged over the study region Δ (see bold black contour in Figure 2b). (b) As in (a) except for the Δ-averaged monthly surface evaporation *E* (mm/day). (c) As in (a) except for the monthly discharge *Q* (mm/day) at Kienstock (see location in Figure 2b). In the case of WRF, *Q* is evaluated with the Δ-averaged runoff *R*, that is, the sum of surface and underground runoff. WRF = Weather Research and Forecasting.

The annual cycle of surface evaporation is well captured by both models, with some overestimation during the winter months and underestimation during the spring and autumn months. Annually, WRF overestimates E_{OBS} by 2.7 mm/year (+0.6%) and WRF-Hydro by 7.3 mm/year (+1.5%). The slight increase in surface evaporation induced by WRF-Hydro is the consequence of ponded water infiltration, which increases the soil water storage, as discussed by, for example, Senatore et al. (2015), Arnault et al. (2018), Rummler et al. (2019), and Zhang et al. (2019).

Strikingly, the monthly variation of Δ-averaged runoff in WRF matches the monthly variation of discharge at Kienstock in WRF-Hydro and is close to the observation. This demonstrates the ability of both WRF and WRF-Hydro in closing the Δ-averaged terrestrial water balance at the monthly time scale. The modeled total runoff and discharge are generally underestimated with an annual difference to observation of −19.1 mm/year (−3.3%) for WRF and −24.0 mm/year (−4.1%) for WRF-Hydro. This negative bias could be related to groundwater dynamics, which is well captured neither by the Δ-averaged underground runoff in WRF nor by the groundwater bucket and pass-through option in WRF-Hydro. The slight decrease in annual discharge in WRF-Hydro is related to the above-discussed slight increase in annual surface evaporation caused by the ponded water infiltration.

Daily time series of Δ-averaged P_{WRF}, $P_{WRF\ -\ Hydro}$, and P_{OBS} are displayed in Figure 4. The time series of Figure 4a have been filtered with a 7-day moving average filter for visualization purpose. The unfiltered WRF and WRF-Hydro time series are close, each with a correlation to observation of 0.87 for the period 1 January 2008 to 31 December 2011. This demonstrates the skill of the WRF and WRF-Hydro setups of section 3.1 in reproducing daily variations of the Δ-averaged precipitation product.

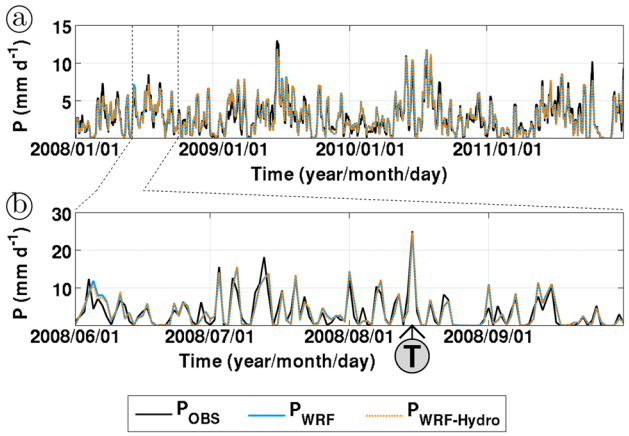

Figure 4. (a) Daily time series of Δ-averaged daily precipitation P (mm/day) from the observational data set, WRF and WRF-Hydro, filtered with a 7-day moving average filter. (b) As is (a) except for the unfiltered daily precipitation during the period June–September 2008. The circled symbol "T" indicates the selected event for the source precipitation on which the soil-vegetation-atmospheric water tagging procedure of section 2 is applied.

At the daily scale, the observed discharge at Kienstock is also approximately well reproduced by our WRF-Hydro simulation, as displayed in Figure 5, with a correlation of 0.76 and a Kling-Gupta efficiency (Gupta et al., 2009) of 0.66. Differences between modeled and observed discharge are related to (1) discrepancies in the spatial distribution of modeled precipitation, (2) potential model misrepresentation of soil and land surface processes, and (3) potentially inadequate values of distributed soil and land surface parameters, which are currently assigned as a function of soil classes. Nevertheless, the fact that modeled Δ-averaged precipitation and modeled discharge at the basin outlet give a comparably high correlation to daily observation demonstrates the skill of the WRF and WRF-Hydro setups of section 3.1 in realistically representing observed water fluxes in the study region. This suggests that these model setups also have the potential to realistically represent the water pathways of a given source of water through the terrestrial and atmospheric water compartments in the study region. We therefore state that these model setups are suitable for investigating the contribution of lateral terrestrial water flow to the regional hydrological cycle occurring in the area of the upper Danube river basin with the SVA-TAG procedure of section 2.

3.3. Precipitation Tagging Setup

The SVA-TAG procedure of section 2 is now applied to the source precipitation defined as the precipitation falling in Δ between 1200 UTC 14 August 2008 and 1800 UTC 16 August 2008. This period of tagging event was selected as it corresponds to one of the wettest events of the summer 2008 (see Figure 4b). The exact start and end dates of the tagging period have been chosen in order to cover the entire event in the simulation.

The first objective is to investigate the fate of this source precipitation in the simulated regional hydrological cycle with WRF-tag and with WRF-Hydro-tag, until the end of the simulation in December 2011. The second objective is to assess the contribution of lateral terrestrial water flow to the fate of this source precipitation.

Technically, the WRF and WRF-Hydro 5-year simulations of section 3.1 are reconducted using the model versions enhanced with the SVA-TAG procedure, namely, WRF-tag and WRF-Hydro-tag. Tagged water variables are initialized to 0, and the source precipitation is set as the precipitation falling in Δ during the tagging period. Traditional three-dimensional terrestrial and atmospheric water variables, their tagged counterparts, and the two-dimensional terms of the budgets of tagged terrestrial water and tagged atmospheric water, namely, equations (8) and (17), are saved in the model outputs.

4. Tagging Results and Discussions

4.1. Characteristics of Total Water Fluxes During the Tagging Period

Tagged water is part of the total water, so that the knowledge of the processes acting on total water can help understanding the processes acting on tagged water. For this purpose, this section aims at presenting the characteristics of the total water fluxes during the tagging period.

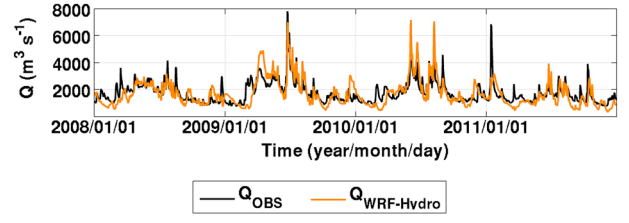

Figure 5. Daily time series of daily discharge Q (m^3/s) at Kienstock from the gauge observation and WRF-Hydro.

Figure 6 provides maps of $W_{\theta,0-100}$, which is the total soil moisture content between 0- and 100-cm depths, and $W_{\theta,100-200}$, which is the total soil moisture content between 100-and 200-cm depths, averaged for the tagging period. The maps of the left column are from WRF-tag, whereas the maps of the right column are from the difference between WRF-tag and WRF-Hydro-tag. The southern subregion Δ_1 and the northern subregion Δ_2 are also indicated in Figure 6 in order to analyze the respective effects of lateral terrestrial water flow and topography on total soil moisture and total water fluxes. In WRF-tag, during the tagging period, $W_{\theta,0-100}$ and $W_{\theta,100-200}$ show similar spatial patterns, with enhanced amounts in Δ_2. This is related to larger precipitation amounts generally

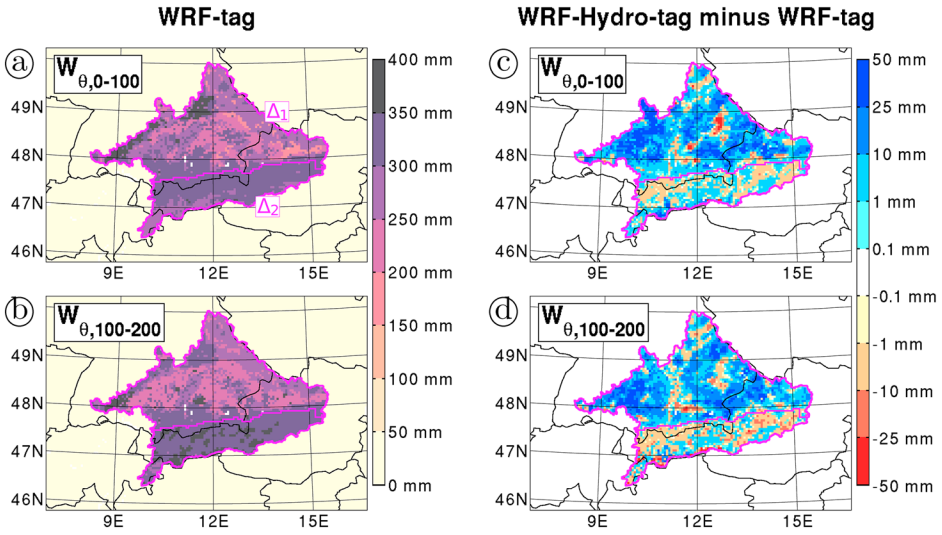

Figure 6. (a) Map of $W_{\theta,0-100}$ (mm) that is the total soil moisture content between 0- and 100-cm depths, averaged for the tagging period between 1200 UTC 14 August 2008 and 1800 UTC 16 August 2008, derived from WRF-tag. The location of the subregions Δ_1 and Δ_2 is indicated by the bold magenta contour. (b) As in (a) except for $W_{\theta,100-200}$ (mm) that is the total soil moisture content between 100- and 200-cm depths. (c and d) as in (a) and (b) except for the difference between WRF-tag and WRF-Hydro-tag. WRF = Weather Research and Forecasting.

occurring in the Alpine region. In comparison to WRF-tag, WRF-Hydro-tag predicts drier soils in the steep topography subregion Δ_2 and wetter soils in the moderate topography subregion Δ_1.

Figure 7 provides maps of the total water fluxes from WRF-tag (a–d) and from the difference between WRF-tag and WRF-Hydro-tag (e–h), accumulated for the tagging period. In WRF-tag the precipitation generated during the tagging period, previously referred as P^{source}, covers the entire study region Δ, with enhanced amounts over the highest mountain ranges in Δ_2. The spatial patterns of the WRF-tag total surface runoff follow the spatial patterns of P^{source}, which is coherent with the fact that in the Noah LSM the surface runoff is computed as the part of the precipitation which does not infiltrate. The high amounts of surface runoff occurring at the highest elevations are related to snowmelt. The WRF-tag total underground runoff is rather located in Δ_2, in relation with the above-discussed enhanced total soil moisture, whereas the WRF-tag total surface evaporation occurs all over Δ.

In comparison to WRF-tag, WRF-Hydro-tag generates slightly different spatial patterns of P^{source}, which, however, do not directly affect the differences in total surface runoff, total underground runoff and total surface evaporation between WRF-tag and WRF-Hydro-tag during the tagging period, as displayed in Figures 7e–7h. The WRF-Hydro-tag induced changes in total surface runoff and total underground runoff are rather related to topography. In particular, WRF-Hydro-tag generates more total surface runoff and less total underground runoff in Δ_2 but less total surface runoff and more total underground runoff in Δ_1. This is related to the more realistic description of the surface runoff generation mechanism in WRF-Hydro, which is more efficient in steep topography gradient areas. Indeed, the subsurface lateral water flow accumulates total soil moisture toward valley bottoms. In steep terrain this generates total exfiltration in association with soil drying, whereas in moderate terrain this increases the total underground runoff in association with soil wetting, as shown in Figures 6c and 6d. Consequently, WRF-Hydro-tag mainly enhances total surface evaporation in Δ_1 (see Figure 7h), which is in agreement with the slight increase in annual surface evaporation in WRF-Hydro previously discussed in section 3.2.

4.2. Horizontal Distribution of Tagged Soil Moisture

Precipitation tagging results are qualitatively assessed with the maps of $W^{tagged}_{\theta,0-100}$, which is the tagged soil moisture content between 0 and 100 cm depth, and $W^{tagged}_{\theta,100-200}$, which is the tagged soil moisture content between 100- and 200-cm depths, displayed for 1 September 2008, 1 September 2009, and 1 September

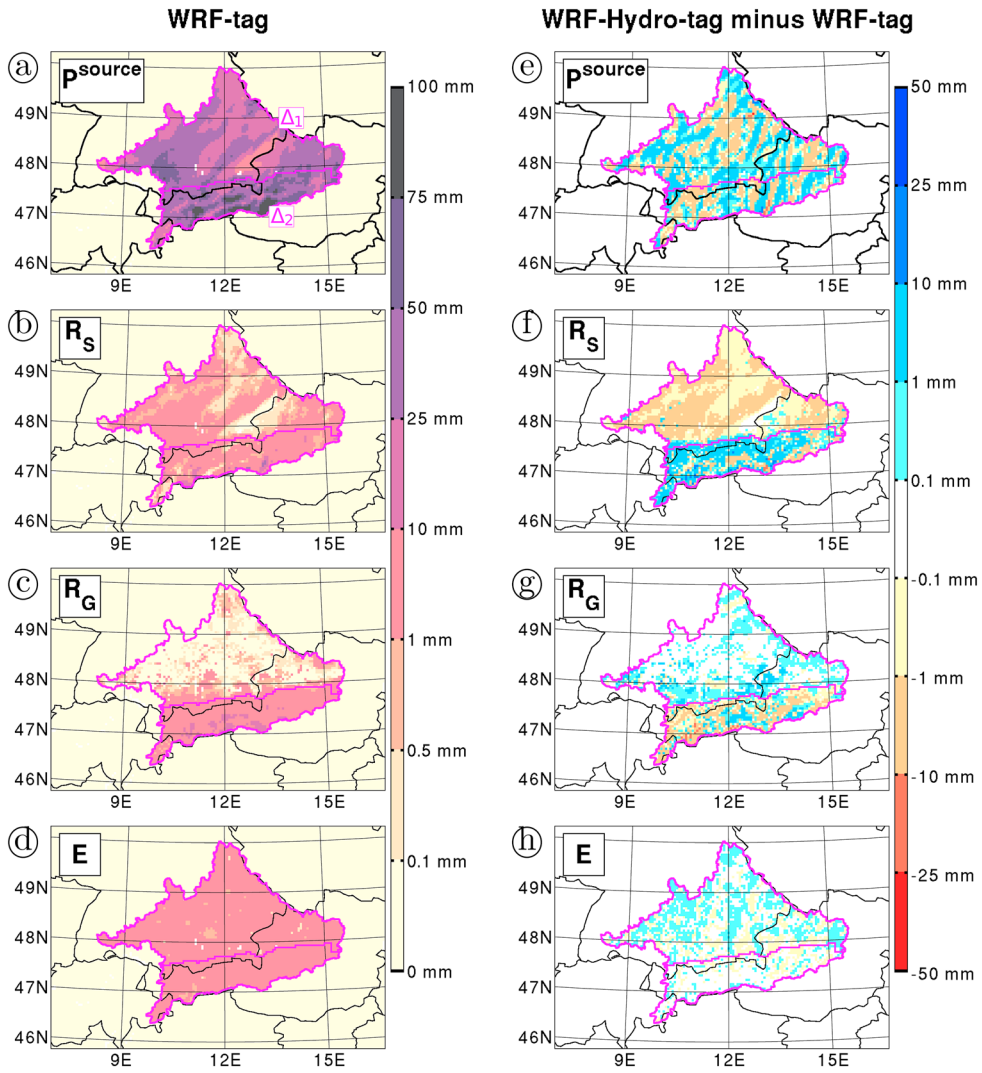

Figure 7. (a–d) Maps of accumulated total water fluxes (mm) for the tagging period between 1200 UTC 14 August 2008 and 1800 UTC 16 August 2008, namely, source precipitation P^{source}, total surface runoff R_S, total underground runoff R_G, and total surface evaporation E, derived from WRF-tag. (e–h) As in (a)–(d) except for the difference between WRF-Hydro-tag and WRF-tag. WRF = Weather Research and Forecasting.

2010 in Figures 8–10, respectively. As in Figures 6 and 7, panels (a) and (b) in Figures 8–10 show the WRF-tag result, whereas the right column shows the differential result between WRF-tag and WRF-Hydro-tag. The two subregions Δ_1 and Δ_2 are also indicated in Figures 8–10 in order to analyze the respective effects of lateral terrestrial water flow and topography on the tagged soil moisture horizontal distribution.

On 1 September 2008, which is 15 days after the end of the tagging period, the tagged soil moisture in both WRF-tag and WRF-Hydro-tag is mainly confined between 0- and 100-cm depths, with spatial patterns close to the spatial patterns of P^{source} (Figure 8). In WRF-tag, some infiltration of tagged soil moisture below 100-cm depth has already occurred at this date, especially in Δ_2 where P^{source} is enhanced. In WRF-Hydro-tag, the infiltration of tagged ponded water increases the amount of tagged soil moisture, which can be seen in Δ_1 for $W^{tagged}_{\theta,0-100}$ and in Δ_2 for $W^{tagged}_{\theta,100-200}$. Concerning $W^{tagged}_{\theta,0-100}$ in Δ_2, the effect of tagged ponded water infiltration is counterbalanced by the tagged exfiltration, which is enhanced in steep topography gradient areas.

One year later, which is on 1 September 2009, $W^{tagged}_{\theta,0-100}$ has largely been removed in Δ_2 but not in Δ_1 in both WRF-tag and WRF-Hydro-tag, as displayed in Figure 9. Indeed, as noticed by Sprenger et al. (2016), the

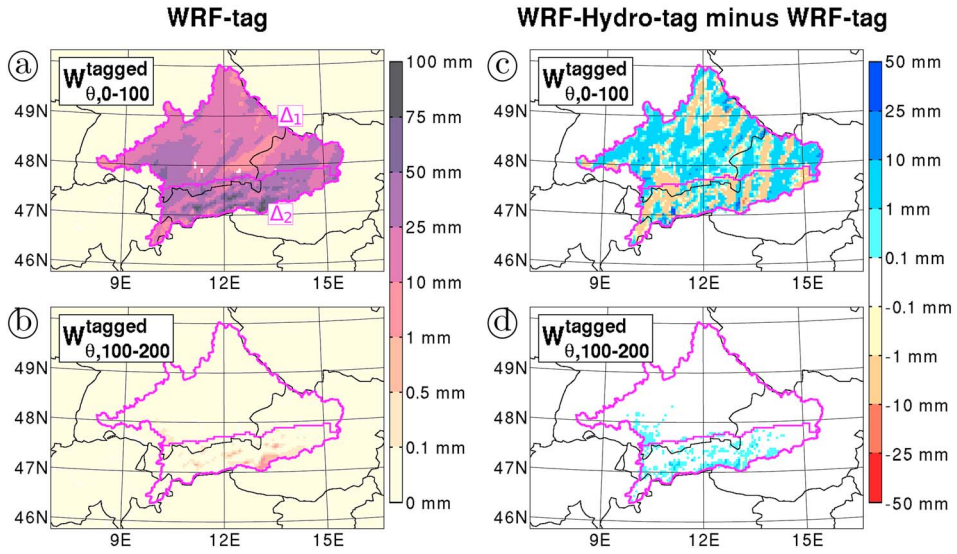

Figure 8. (a and b) Map of $W^{tagged}_{\theta,0-100}$ (mm) that is the tagged soil moisture content between 0- and 100-cm depths, at 0000 UTC on 1 September 2008, derived from WRF-tag. (b) As in (a) except for $W^{tagged}_{\theta,100-200}$ (mm) that is the tagged soil moisture content between 100- and 200-cm depths. (c and d) As in (a) and (b), except for the difference between WRF-tag and WRF-Hydro-tag. WRF = Weather Research and Forecasting.

travel time of precipitated water in the root zone is mainly driven by subsequent precipitation amounts. Hence, the infiltration of $W^{tagged}_{\theta,0-100}$ to lower soil layers is quicker in Δ_2 which receives more precipitation, except for the highest elevation parts which experience a sufficiently long lasting soil freezing to block infiltration. In comparison to WRF-tag on 1 September 2009, the value of $W^{tagged}_{\theta,0-100}$ in WRF-Hydro-tag is higher in Δ_2, and lower in Δ_1. Contrarily, the value of $W^{tagged}_{\theta,100-200}$ in WRF-Hydro-tag is lower in some parts of Δ_2 and mainly higher in Δ_1. Indeed, for steep terrain such as Δ_2 the tagged subsurface lateral water flow in WRF-Hydro-tag generates tagged exfiltration, which tends to accumulate tagged soil moisture in the upper layers. Whereas for moderate terrain such as Δ_1 the tagged subsurface lateral water flow rather accumulates tagged soil moisture in the lower soil layers. As a side note, the fact that for some high

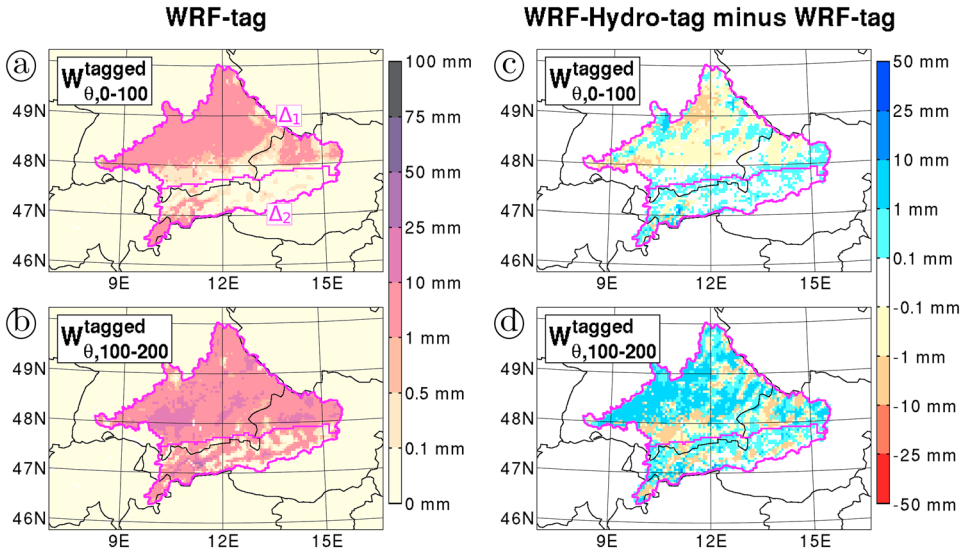

Figure 9. As in Figure 8 except on 1 September 2009.

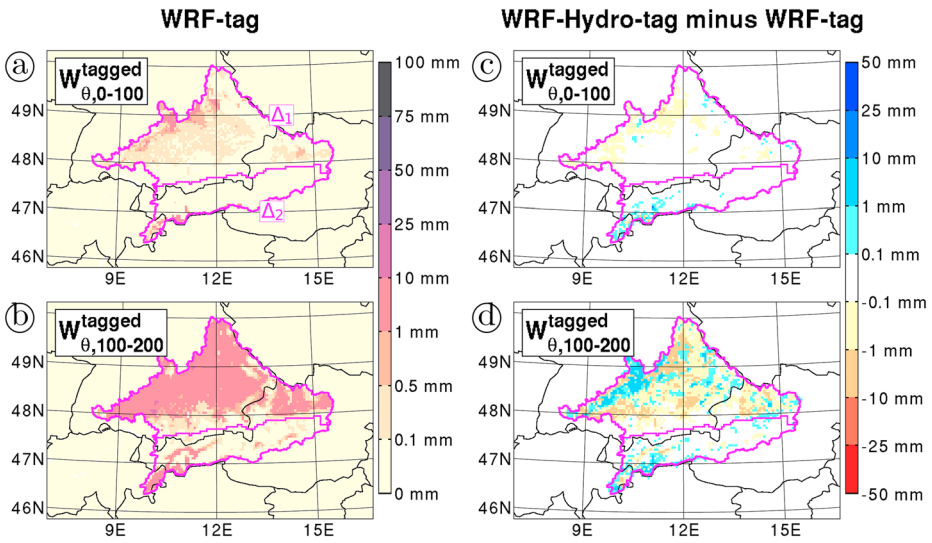

Figure 10. As in Figure 8 except on 1 September 2010.

elevation parts $W^{tagged}_{\theta,100-200}$ on 1 September 2009 remains much higher in WRF-Hydro-tag than in WRF-tag is related to locally enhanced P^{source} and enhanced infiltrated amounts, leading to a slower depletion of tagged soil moisture in WRF-Hydro-tag at these locations. The contribution of tagged snowmelt to tagged ponded water infiltration at the high elevation parts (see equations (3) and (9)) also contributes to this tagged soil moisture enhancement in WRF-Hydro-tag.

Two years later, which is on 1 September 2010, most of $W^{tagged}_{\theta,0-100}$ has been depleted in both WRF-tag and WRF-Hydro-tag, as displayed in Figure 10. In Δ_2 $W^{tagged}_{\theta,100-200}$ has also been mainly depleted, except for the parts which experience a sufficiently long lasting soil freezing, as previously mentioned. In comparison to WRF-tag on 1 September 2010, the value of $W^{tagged}_{\theta,100-200}$ in WRF-Hydro-tag is slightly lower in Δ_1, which is related to the enhancement of tagged underground runoff in moderate terrain (see next section).

4.3. Horizontal Distribution of Tagged Water Fluxes

In order to complement the above analysis of tagged soil moisture, maps of tagged water fluxes from equations (8) and (17) are accumulated for the whole study period and shown in Figure 11. As in Figures 6–10, the left column of Figure 11 shows the WRF-tag result, whereas the right column shows the differential result between WRF-tag and WRF-Hydro-tag. In the WRF-tag simulation, the tagged surface runoff, tagged underground runoff, and tagged surface evaporation, previously referred to as R_S^{tagged}, R_G^{tagged}, and E^{tagged}, respectively, cover the entire study region Δ and display spatial patterns close to those in P^{source} (Figure 7a). Noticeably, R_S^{tagged} accumulated for the whole study period in Figure 11a is nearly identical to the total surface runoff accumulated for the tagging period in Figure 7b, except for the snowmelt parts. This is related to the fact that in WRF-tag the tagged surface runoff is almost entirely generated when source precipitation occurs (see also equation (5)).

In the WRF-tag simulation, R_G^{tagged} accumulated for the whole study period in Figure 11b shows not only enhanced values in Δ_2, as with the total underground runoff accumulated for the tagging period in Figure 7c, but also much larger values in Δ_1. Indeed, the root zone transit time of tagged soil moisture is larger in Δ_1 than in Δ_2 in relation with enhanced precipitation amounts in the Alpine region (Δ_2), as mentioned above (Sprenger et al., 2016). Accordingly, the accumulation for the whole study period allows to display the tagged underground runoff in Δ_1, which takes a longer lapse of time to be generated. The tagged precipitation, previously referred to as P^{tagged} (see equation (17)), is comparatively much smaller, with enhanced values in Δ_2, as displayed in Figure 11d. This suggests that the mountainous part of the basin has a blocking effect on the tagged atmospheric water.

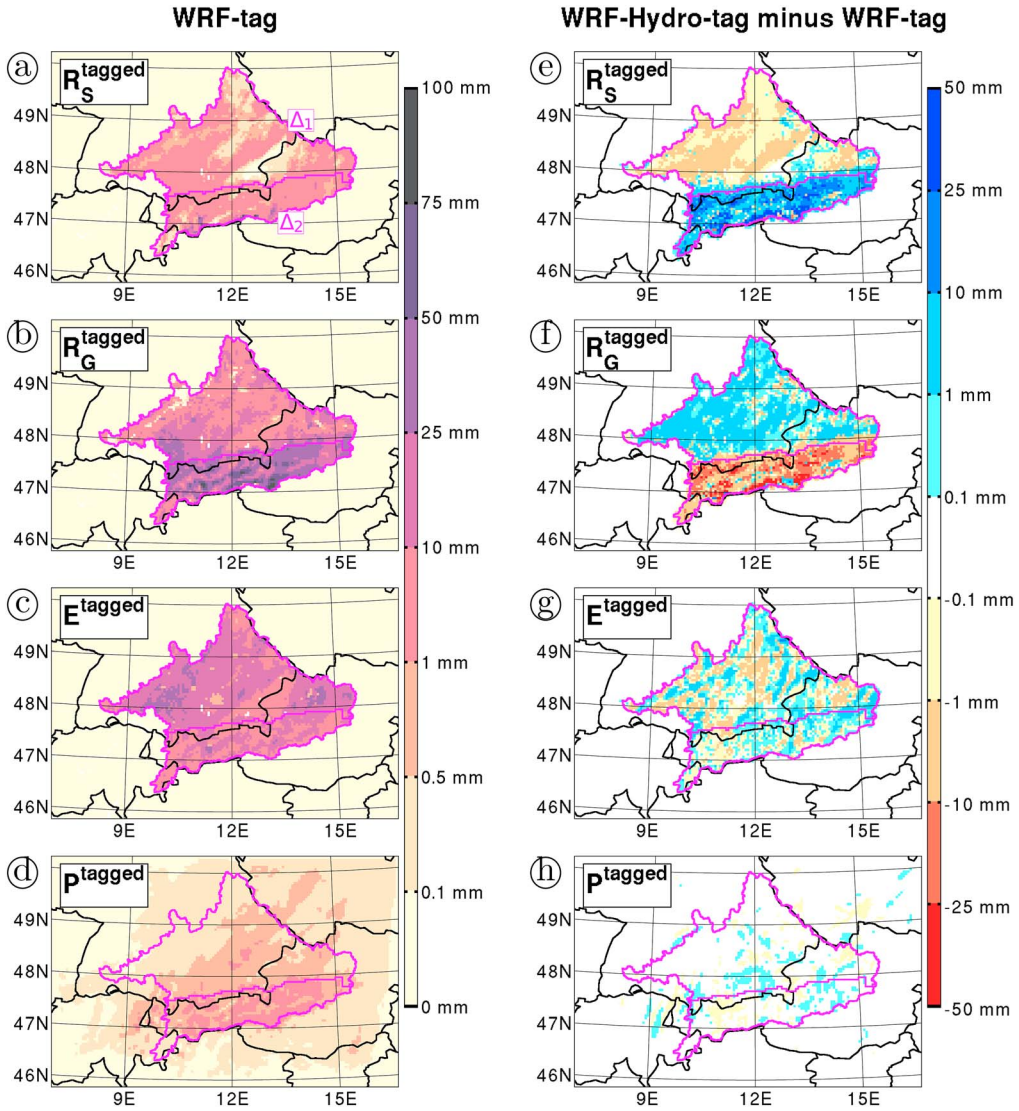

Figure 11. (a–d) Maps of accumulated tagged water fluxes (mm) for the whole study period from 1 January 2008 to 31 December 2011, namely, tagged surface runoff R_S^{tagged}, tagged underground runoff R_G^{tagged}, tagged surface evaporation E^{tagged}, and tagged precipitation P^{tagged}, derived from WRF-tag. (e–h) As in (a)–(d) except for the difference between WRF-Hydro-tag and WRF-tag. WRF = Weather Research and Forecasting.

In comparison to WRF-tag, WRF-Hydro-tag generates slightly different spatial patterns of P^{source}, which directly affect E^{tagged}. This contributes to the small differences in P^{tagged} displayed in Figure 11h. The WRF-Hydro-tag induced changes in R_S^{tagged} and R_G^{tagged} rather follow the WRF-Hydro-tag induced changes in total surface runoff and total underground runoff previously described in section 4.1 (cf. Figures 11e and 11f with Figures 7f and 7g). In particular, WRF-Hydro-tag generates much more R_S^{tagged} and much less R_G^{tagged} in Δ_2 but slightly less R_S^{tagged} and slightly more R_G^{tagged} in Δ_1. This effect of WRF-Hydro-tag on R_S^{tagged} and R_G^{tagged} is attributed to the tagged subsurface lateral water flow, which either generates tagged exfiltration and increases R_S^{tagged} in steep terrain or accelerates the infiltration of tagged soil moisture and increases R_G^{tagged} in moderate terrain. Indeed, the tagged surface lateral water flow increases the tagged infiltration area toward valley bottoms. For the case of moderate terrain where the topography gradients are not steep enough to generate tagged exfiltration, the expansion of the tagged infiltration area leads to an acceleration of the tagged infiltration.

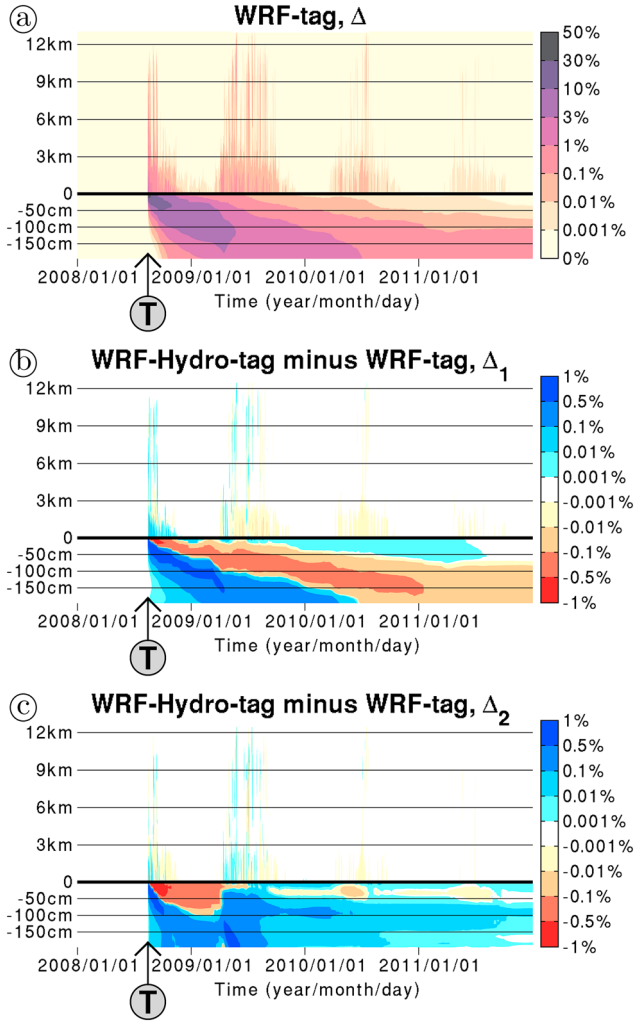

Figure 12. (a) Time-height diagram of tagged soil and atmospheric water ratio (%), spatially averaged over the study region Δ at a daily time scale, derived from WRF-tag. The *x* axis gives the time from 1 January 2008 to 31 December 2011, with the circle symbol "T" indicating the period of the source precipitation from which the tagged water originates. The bold horizontal line indicates the surface, and the *y* axis gives the average height above (below) the surface in kilometers (cm). (b) As in (a) except for the difference between WRF-Hydro-tag and WRF-tag spatially averaged over the subregion Δ_1. (c) As in (a) except for the difference between WRF-Hydro-tag and WRF-tag spatially averaged over the subregion Δ_2. WRF = Weather Research and Forecasting.

4.4. Vertical Distribution of Tagged Water

Precipitation tagging results are further qualitatively assessed with the time-height diagrams of spatially averaged tagged soil and atmospheric water ratio in Figure 12, which allows to jointly visualize the fate of the tagged water in the soil and atmospheric water compartments. In this figure, the tagged soil water ratio is defined as the tagged soil moisture ratio, which is the ratio between tagged and total soil moisture, whereas the tagged atmospheric water ratio is defined as the ratio between tagged and total atmospheric water. Also, the plotted data are daily averaged in order to mask the diurnal cycle. More particularly, Figure 12a displays the Δ-averaged tagged water from WRF-tag for the whole study period from 1 January 2008 to 31 December 2011. Figures 12b and 12c display the difference between WRF-tag and WRF-Hydro-tag results for the Δ_1 and Δ_2 subregions, in order to further analyze the respective effects of lateral terrestrial water flow and topography on the vertical distribution of tagged water.

In the WRF-tag simulation, the tagged water infiltrates and partially fills the 2 m of soil within a few weeks, as shown by the profile of tagged moisture ratio in Figure 12a. We find that 12% of the tagged water evaporates during the first 10 days following the beginning of the tagging period in the WRF-tag simulation, which contributes to the convective systems occurring in the study region and generates the plumes of enhanced tagged atmospheric water displayed in Figure 12a. During the week following the tagging event, these plumes are characterized by tagged atmospheric water ratio values above 1% in the lower tropospheric levels and above 0.1% in the midtropospheric levels.

We find that in WRF-tag the tagged soil moisture ratio at a depth of 1 m reaches its maximum of 6.5% at the beginning of March 2009, whereas the tagged soil moisture ratio at a depth of 2 m reaches its maximum of 2.8% 2 months later. Afterward, the tagged soil moisture ratio decreases in all layers, especially during the warm months when E^{tagged} is enhanced. Accordingly, the tagged atmospheric water ratio is also enhanced during the warm months, with a decrease from year to year. Three years after the tagging period, in 2011, the tagged atmospheric water ratio, as well as the tagged soil moisture ratio in the first 50 cm of soil, is generally below 0.01%.

In comparison to WRF-tag, at the end of the tagging period WRF-Hydro-tag has increased the tagged soil moisture ratio in the first 50 cm of soil by +0.1 to +1%, as shown in Figures 12b and 12c. Indeed, as already mentioned, the additionally resolved lateral terrestrial water flow in WRF-Hydro-tag allows for the source precipitation to partly remain at the surface as tagged ponded water, which consequently increases the amount of tagged soil infiltration and tagged soil moisture. However, quickly after the end of the tagging period, the tagged soil moisture ratio in the upper soil layers decreases faster in WRF-Hydro-tag than in WRF-tag. This means that the washing out of precipitated water by subsequent precipitation amounts described by Sprenger et al. (2016) is accelerated by the description of lateral terrestrial water flow, through enhanced tagged infiltration in moderate terrain such as Δ_1, and enhanced tagged exfiltration in steep terrain such as Δ_2.

In Δ_1, the near-surface layer of depleted tagged soil moisture in WRF-Hydro-tag widens, propagates downward, and reaches the soil bottom at 2-m depth after a 2-year period, as shown in Figure 12b. During that 2-year period, the Δ_1-averaged tagged soil moisture ratio in the lower soil layers of WRF-Hydro-tag remains larger than in WRF-tag, which is in correspondence with the above-discussed increased amount of tagged soil infiltration during the tagging period in WRF-Hydro-tag. From 2009 on, the fact that

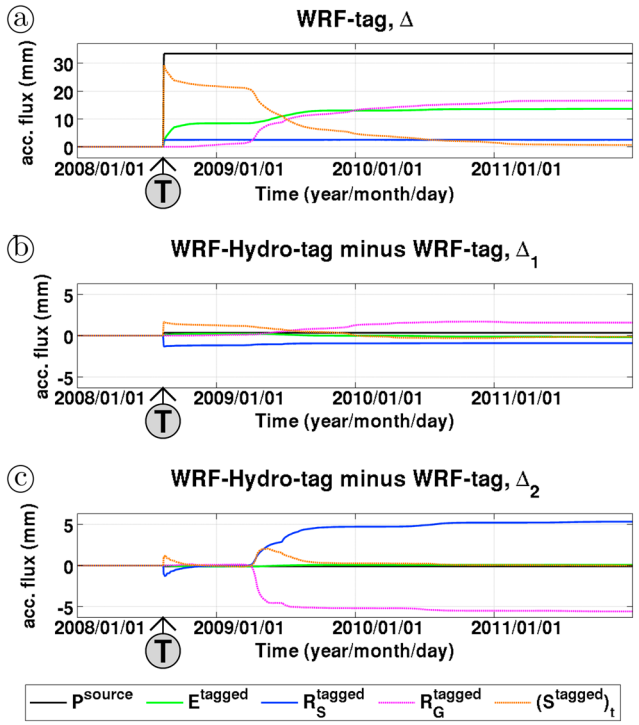

Figure 13. (a) Daily time series of the tagged terrestrial water fluxes from the budget equation (8) derived from WRF-tag, spatially averaged over the study region Δ and displayed as daily accumulated sums (mm) from 1 January 2008 to 31 December 2011. P^{source}, E^{tagged}, R_S^{tagged}, R_G^{tagged}, and $(S^{tagged})_t$ stand for source precipitation, tagged surface evaporation, tagged surface runoff, tagged underground runoff and change in tagged terrestrial water storage, respectively. (b) As in (a) except for the difference between WRF-Hydro-tag and WRF-tag spatially averaged over the subregion Δ_1. (c) As in (a) except for the difference between WRF-Hydro-tag and WRF-tag spatially averaged over the subregion Δ_2. WRF = Weather Research and Forecasting.

in Δ_1 the tagged soil moisture in the upper soil layers in WRF-Hydro-tag becomes again slightly larger than in WRF-tag is related to exfiltration of tagged soil moisture from lower soil layers to upper soil layers and a weak generation of tagged surface runoff in Δ_1 (see section 4.5.3 and Figure 13b). In Δ_2 the tagged exfiltration is much enhanced by the steep topography gradients, so that from mid-2009 on the tagged soil moisture in the upper soil layers in WRF-Hydro-tag becomes again larger than in WRF-tag, as shown in Figure 12c. As a consequence, from mid-2009 on the previously discussed WRF-Hydro-tag induced layer of depleted tagged soil moisture almost disappears in Δ_2.

Concerning the atmospheric water compartment, WRF-Hydro-tag slightly enhances the ratio of tagged atmospheric water mainly during the few weeks following the tagging event, up to +0.1%, and slightly reduces this ratio afterward, up to −0.01%, in both subregions Δ_1 and Δ_2. This is related to the effect of WRF-Hydro-tag on tagged soil moisture and E^{tagged}, which is discussed in details in the following section.

4.5. Budgets and Transit Time

Precipitation tagging results are quantitatively assessed with the budget equations (8) and (17) of tagged terrestrial water and tagged atmospheric water, respectively. Figures 13 and 14 display the spatially averaged terms of these budgets as daily accumulated time series from 1 January 2008 to 31 December 2011. In particular, Figures 13a and 14a display the Δ-averaged budgets from WRF-tag, whereas Figures 13b, 13c, 14b, and 14c further display the differences in the Δ_1-averaged budgets and Δ_2-averaged budgets between WRF-tag and WRF-Hydro-tag, with the aim to analyze the respective effects of lateral terrestrial water flow and topography on water transit time. Sums for the 4-year period are provided in Table 1.

For the selected tagging event, WRF-Hydro-tag produces 0.5% more Δ-averaged P^{source} than WRF-tag. This difference in precipitation amount for a selected event is related to differences in atmospheric circulation between the WRF-tag and WRF-Hydro-tag simulations. Nevertheless, it is assumed that the precipitation partitioning processes of P^{source} in the two models can be compared.

4.5.1. Tagged Terrestrial Water in WRF-tag

In the WRF-tag simulation, most R_S^{tagged} occurs during the tagging period, as shown in Figure 13a. The tagged water which infiltrates is temporarily stored in the 2 m of soil depth, and is slowly depleted through E^{tagged} and R_G^{tagged}. At the end of the WRF-tag simulation, approximately 1.9% of the tagged water remains in the soil, while 57.2% has run off and 40.9% has evaporated back to the atmosphere (Table 1).

In comparison to Hu et al.'s (2018) result obtained for an extreme precipitation event at the beginning of the cold season in the U.S. Pacific Northwest, we find that, in our simulation, the amount of tagged water remaining in the soil at the end of the tagging event is 85%, the other 15% being approximately equally distributed among surface runoff and surface evaporation. On the other hand, Hu et al. (2018) found that only 66% of their tagged water was in the soil at the end of their tagging event, as 29% also went to the snow storage in their case. Furthermore, after a 6-month period, Hu et al. (2018) found that the amount of tagged water in the soil decreased to 53% with the complete mixing assumption and to 30% when relaxing this assumption, which gives a reduction between −13% and −36%. In our case, with the complete mixing assumption, we find that the amount of tagged water in the soil decreases to 64% after a 6-month period, which corresponds to a reduction by −21%. Relaxing the complete mixing assumption would certainly accelerate the depletion of tagged water from the soil, although, similar to Hu et al. (2018), we do not have observational products of transit time at the scale of our study region to validate the benefit of relaxing this assumption.

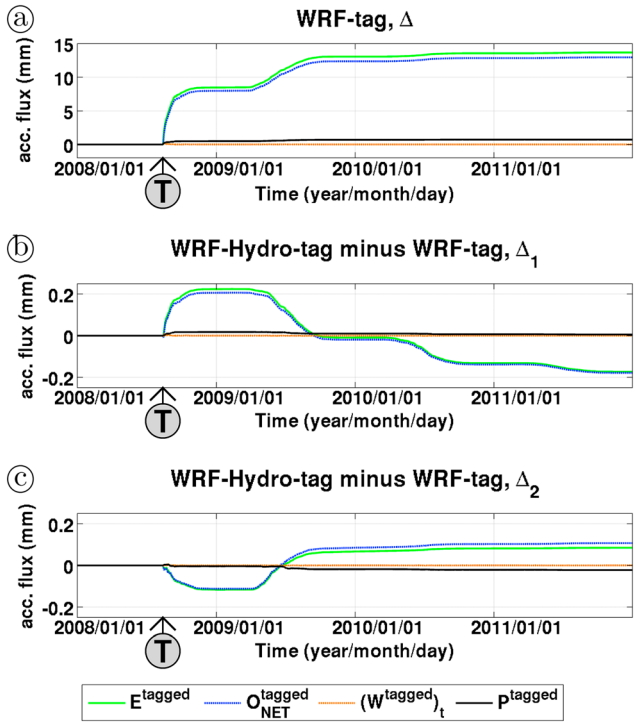

Figure 14. (a) Daily time series of the tagged atmospheric water fluxes from the budget equation (17) derived from WRF-tag, spatially averaged over the study region Δ and displayed as daily accumulated sums (mm) from 1 January 2008 to 31 December 2011. E^{tagged}, O_{NET}^{tagged}, $(W^{tagged})_t$, and P^{tagged} stand for tagged surface evaporation, net outflow of tagged atmospheric water, change in tagged atmospheric water and tagged precipitation, respectively. (b) As in (a) except for the difference between WRF-Hydro-tag and WRF-tag spatially averaged over the subregion Δ_1. (c) As in (a) except for the difference between WRF-Hydro-tag and WRF-tag spatially averaged over the subregion Δ_2. WRF = Weather Research and Forecasting.

4.5.2. Tagged Atmospheric Water in WRF-tag

In the WRF-tag simulation, E^{tagged} is enhanced during the warm months (see Figure 14a). During the weeks following the tagging event in 2008, E^{tagged} is mostly the result of tagged canopy water evaporation, tagged direct evaporation and tagged plant transpiration, as the sublimation of the tagged snow received at the high elevations of the upper Danube river basin has a rather small contribution at basin scale (not shown). However, the tagged canopy water and tagged soil moisture in the first soil layer are quickly depleted, so that E^{tagged} occurring during the years 2009–2011 is primarily due to tagged plant transpiration, which pumps tagged soil moisture from lower soil layers.

Table 1
Partitioning of the Source Precipitation, Having Fallen in the Upper Danube River Basin (See Bold Black Contour in Figure 1b) From 1200 UTC 14 August 2008 to 1800 UTC 16 August 2008, Among the Terrestrial and Atmospheric Water Compartments, at the End of the WRF/WRF-Hydro Simulations on 31 December 2011

Water flux	WRF	WRF-Hydro
Source precipitation	33.5 mm	33.6 mm
Soil storage	1.9%	1.6%
Surface runoff	7.5%	16.8%
Underground runoff	49.7%	41.1%
Evapotranspiration (atmospheric transport and recycled precipitation)	40.9% (38.8, 2.1%)	40.5% (38.4, 2.1%)

Note. WRF = Weather Research and Forecasting.

In the atmosphere, E^{tagged} contributes to the precipitation occurring in Δ during the tagging period and subsequent precipitation events during the warm months, although most of the tagged evaporated water produced during the simulation is advected outside of the lateral boundaries of the source region, as diagnosed in Figure 14a. Indeed, as pointed out by Van der Ent and Savenije (2011), length scales of atmospheric water motions are usually larger than 2,000 km in temperate climates, which is much larger than the source region considered in this study with a size of approximately 500 km × 200 km.

4.5.3. Effect of WRF-Hydro-tag on Tagged Terrestrial Water

In comparison to WRF-tag, WRF-Hydro-tag produces less R_S^{tagged} during the tagging event and increases the amount of tagged soil moisture storage in both subregions Δ_1 and Δ_2, as shown in Figures 13b and 13c.

In Δ_1 the excess of tagged soil moisture in WRF-Hydro (see Figure 13b) is slightly depleted by E^{tagged} in 2008. In 2009 and 2010, this excess of tagged soil moisture is mostly depleted by R_G^{tagged} and to a much lower extend by R_S^{tagged} as well. From 2010 on the Δ_1-averaged tagged soil moisture amount in WRF-Hydro-tag becomes smaller than that in WRF-tag. This is related to the WRF-Hydro-tag induced increase in R_G^{tagged} in Δ_1 discussed in section 4.3 (see Figure 11f) and confirms that the tagged subsurface lateral water flow in moderate terrain accelerates the infiltration of tagged soil moisture.

In Δ_2 the excess of tagged soil moisture in WRF-Hydro (see Figure 13c) is mostly depleted by R_S^{tagged} in 2008, which confirms that the relative decrease in tagged soil moisture in the upper soil layer in WRF-Hydro-tag, in comparison to WRF-tag, is related to tagged surface runoff generation (see sections 4.4 and Figure 12c). In 2009, R_G^{tagged} is delayed in comparison to R_S^{tagged}, which results in a transient enhancement of tagged soil moisture in WRF-Hydro-tag in comparison to WRF-tag, as displayed in Figure 13c. The delayed production of R_S^{tagged} in Δ_2 in WRF-Hydro-tag is mostly counterbalanced by a reduction of R_G^{tagged}, as displayed in Figures 11e, 11f, and 13c and Table 1.

The above-described result implies that on the one hand, taking into account surface lateral water flow in a LSM increases the transit time of the precipitated water in the root zone by not moving the infiltration excess directly to the surface runoff. However, this transit time increase is reduced in steep topography gradient areas such as Δ_2 where the delayed surface runoff generation also accelerates the depletion of precipitated water from the root zone. On the other hand, taking into account subsurface lateral water flow in a LSM reduces the transit time of precipitated water in the root zone of low topography gradient areas such as Δ_1, where slopes are sufficient to expand the infiltration area of precipitated water toward valley bottoms, but not steep enough to generate exfiltration.

4.5.4. Effect of WRF-Hydro-tag on Tagged Atmospheric Water

The tagged ponded water infiltration in WRF-Hydro-tag enhances E^{tagged} during the tagging period and the following weeks, especially in Δ_1 as shown in Figure 14b. In the case of Δ_2, E^{tagged} is rather reduced in association with the production of R_S^{tagged}, as shown in Figure 14c. Accordingly, Δ_1-averaged P^{tagged} is slightly enhanced, whereas Δ_2-averaged P^{tagged} remains almost unchanged during the tagging period and the following weeks. This WRF-Hydro-tag induced effect on E^{tagged} and P^{tagged}, occurring during and just after the tagging period, is referred to as the primary effect.

During the warm months of 2009–2011, E^{tagged} in Δ_1 is generally lower in WRF-Hydro-tag than in WRF-tag, in relation with the layer of depleted tagged soil moisture in WRF-Hydro-tag occupying a large part of the root zone (see Figure 12b). In Δ_2 this effect is overbalanced by the tagged exfiltration which maintains some tagged soil moisture in the first soil layer and enhanced tagged direct evaporation through all the WRF-Hydro-tag simulation. However, the increase in Δ_2-averaged E^{tagged} in 2009 underbalances the decrease in Δ_1-averaged E^{tagged}, in relation with the much larger area covered by Δ_1, so that both Δ_1-averaged P^{tagged} and Δ_2-averaged P^{tagged} decrease in 2009, as well as in 2010 and 2011. This WRF-Hydro-tag induced effect on E^{tagged} and P^{tagged}, occurring from a few months after the tagging period, is referred to as the secondary effect.

As a side note, the fact that the annual surface evaporation is slightly higher in WRF-Hydro (see section 3.2, and also Senatore et al., 2015, Arnault et al., 2018, Rummler et al., 2019, Zhang et al., 2019) is considered to be related to the primary increasing effect on E^{tagged}, and the relatively high frequency of precipitation events in the study region which masks the secondary decreasing effect on E^{tagged}.

4.6. Source Precipitation Recycling

This section is to evaluate the amount of precipitation from a single event, namely, P^{source}, that recycles in the source region as precipitation. This evaluation is conducted with the source precipitation recycling ratio, defined as the ratio between P^{tagged} and P^{source} spatially averaged over the source region, which in our case is the study region Δ. This ratio is displayed in Figure 15 as a daily time series.

In the WRF-tag simulation, the recycling of P^{source} mostly occurs during the warm months when E^{tagged} is enhanced, mainly in 2008 and in 2009, with a small contribution in 2010 and 2011. More particularly, a large part of this recycling occurs during the first weeks following the event, that is 1.5%, as shown in Figure 15a.

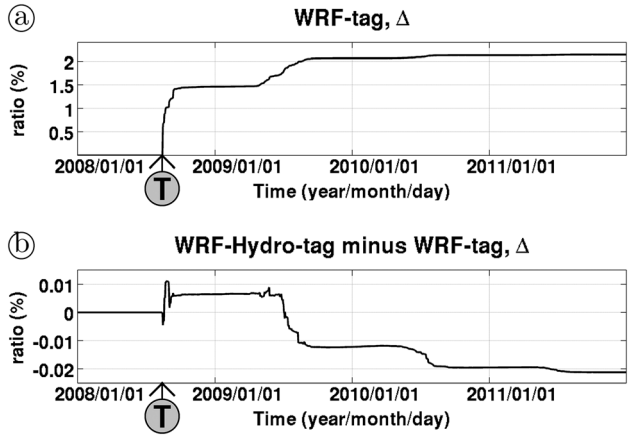

Figure 15. (a) Daily time series of the source precipitation recycling ratio (%) in the study region Δ derived from WRF-tag. (b) As in (a), except for the difference between WRF-Hydro-tag and WRF-tag. WRF = Weather Research and Forecasting.

About +0.6% of recycling occurs in 2009, +0.07% in 2010, and +0.01% in 2011, reaching a total of 2.14% for the entire simulation.

The impact of WRF-Hydro-tag on the source precipitation recycling is small and almost negligible, with an increase reaching +0.01% during the few weeks following the tagging period, followed by a decrease of −0.02% during the year 2009 and −0.01% during the year 2010, as illustrated in Figure 15b.

The effect of WRF-Hydro-tag on the source precipitation recycling can be related to the above defined primary and secondary effects (see section 4.5.4). Primarily, the surface flow infiltration in WRF-Hydro-tag increases the transit time of the precipitated water in the root zone, which increases E^{tagged} and accelerates the recycling of the source precipitation. This primary effect is perturbed by the presence of steep topography gradient areas where the subsurface lateral water flow reduces the transit time of precipitated water in the root zone through surface runoff generation. Secondarily, the subsurface lateral water flow in WRF-Hydro-tag also reduces the transit time of precipitated water in the root zone of the low topography gradient areas through enhanced infiltration, which reduces E^{tagged} and decelerates the source precipitation recycling.

5. Summary and Perspectives

In this study, the evaporation tagging method developed for the regional WRF model by Arnault, Knoche, et al. (2016) has been enhanced with a precipitation tagging method, implemented in the Noah LSM and in the overland and subsurface routing modules of WRF-Hydro. The tagging-enhanced versions of the WRF and WRF-Hydro models have been named as WRF-tag and WRF-Hydro-tag. This so-called joint SVA-TAG procedure allows (1) tracking a source of water through the hydrological compartments resolved in WRF-tag and WRF-Hydro-tag for a limited-area domain and (2) quantifying the contribution of the WRF-Hydro-resolved lateral terrestrial water flow to the hydrological cycle at regional scale.

As a test application, the SVA-TAG procedure was applied to WRF-tag and WRF-Hydro-tag simulations of the precipitation event which occurred in the upper Danube river basin between 1200 UTC 14 August 2008 and 1800 UTC 16 August 2008. This precipitation was considered as water source, tagged and tracked for a 40-month period until December 2011. The consideration of the fate of ponded water in WRF-Hydro-tag enhanced the amount of tagged infiltration during the event, which increased the root zone transit time of the tagged water and slightly increased the tagged surface evaporation and the source precipitation recycling during the few weeks following the tagging event. This effect was reduced in steep topography gradient areas where the enhanced tagged exfiltration counterbalanced the enhanced tagged infiltration. Afterward, the subsurface lateral water flow in WRF-Hydro-tag induced a faster depletion of the tagged soil moisture in low topography gradient areas, thereby decreasing the root zone transit time of the tagged water in these areas, which slightly decreased the tagged surface evaporation and the source precipitation recycling.

The dependency relationship between topography gradients, lateral terrestrial water flow, and precipitation recycling gives a new insight on how the terrestrial and atmospheric branches of the hydrological cycle are connected, which should be further investigated. This is especially relevant for mountainous regions such as the Alps, where a recent study showed that the additional description of lateral terrestrial water flow potentially enhances internal model variability (Rummler et al., 2019).

The reduced impact of lateral terrestrial water flow on tagged surface evaporation obtained in this study may be related to the fact that the study region is located in a humid climate, where soil moisture is not a limiting factor of surface evaporation (e.g., Anyah et al., 2008). Future studies could assess if the consideration of lateral terrestrial water flow in the SVA-TAG procedure would have a larger influence on water pathways in semiarid regions.

A shortage of the precipitation tagging method applied in this study is the simplistic representation of the groundwater dynamics. This could be improved by extending Hu et al.'s (2018) method to the Noah-MP's

groundwater dynamics option from Fan et al. (2007) and Miguez-Macho et al. (2007). The comparison with terrestrial water age observations carried out in catchment transit time research (e.g., Hu et al., 2018; McDonnell et al., 2010; McGuire & McDonnell, 2006) could be used to further evaluate and improve the description of terrestrial water pathways in the model.

It is emphasized that, with a relatively small coding effort, our SVA-TAG procedure can be applied to any water source in the Earth system resolved in WRF-tag and WRF-Hydro-tag. This can potentially bring further new insights to the mechanisms involved in the joint atmospheric-terrestrial hydrological cycle at regional scale, for example, concerning the soil moisture-precipitation feedback (e.g., Duerinck et al., 2016).

To conclude, another innovative aspect of the SVA-TAG procedure is its ability to quantify the impact of modifying terrestrial water pathways on atmospheric water pathways, which is highly relevant for water resources management. Future studies could for example apply the SVA-TAG procedure to land use/land cover change scenario experiments (e.g., Chen & Dirmeyer, 2017) and build a conceptual view of process chain linking a modification of the land surface to a modification in the available water resources.

Appendix A: List of symbols

This appendix provides a list of symbols used the equations of section 2, including the unit and a short description. The symbols are organized in three categories, the first one related to total variables, the second one related to tagged variables, and the last one related to mathematical operators

List of symbols related to total variables

D_θ	(m^2/s)	Soil water diffusivity
Δ_t	(s)	Time step
$\left\{\Delta W_p^{\text{hires}}\right\}_{\text{CR}}$	(m)	Subgrid change of ponded water due to river runoff
Δz_s	(m)	Soil layer thickness
E	(m/s)	Surface evaporation
E_c	(m/s)	Canopy water evaporation
E_s	(m/s)	Surface snow sublimation
I	(m/s)	Surface infiltration
K_θ	(m/s)	Soil hydraulic conductivity
P	(m/s)	Precipitation at the surface
P_{bare}	(m/s)	Water falling on bare soil
$\left\{q_{\text{sfc}}^{\text{hires}}\right\}^{\text{IN}}$	(m)	Subgrid incoming surface lateral water flow
$\left\{q_{\text{sfc}}^{\text{hires}}\right\}^{\text{OUT}}$	(m)	Subgrid outgoing surface lateral water flow
$\left\{q_{\text{sub}}^{\text{hires}}\right\}^{\text{IN}}$	(m)	Subgrid incoming subsurface lateral water flow
$\left\{q_{\text{sub}}^{\text{hires}}\right\}^{\text{OUT}}$	(m)	Subgrid outgoing subsurface lateral water flow
Q	(m/s)	discharge at basin outlet
R	(m/s)	sum of surface runoff and underground runoff
R_{drip}	(m/s)	Canopy water drip
R_G	(m/s)	Underground runoff
R_{melt}	(m/s)	Snowmelt at the land surface
R_S	(m/s)	Surface runoff
σ_f	(−)	Vegetation fraction
θ_{freezing}	(s^{-1})	Rate of freezing liquid soil moisture
θ_{liq}	(−)	Liquid soil moisture
$\theta_{\text{liq}}^{\text{hires}}$	(−)	Subgrid liquid soil moisture
θ_{thawing}	(s^{-1})	Rate of thawing frozen soil moisture
W_p	(m)	Ponded water
W_p^{hires}	(m)	Subgrid ponded water
$W_{\theta,0-100}$	(m)	soil moisture content between 0- and 100-cm depths
$W_{\theta,100-200}$	(m)	soil moisture content between 100- and 200-cm depths

List of symbols related to tagged variables

$\left\{\Delta W_p^{\text{hires,tagged}}\right\}_{\text{CR}}$	(m)	Subgrid change of tagged ponded water due to river runoff
$\left\{\Delta W_p^{\text{hires,tagged}}\right\}_{E}$	(m)	Subgrid change of tagged ponded water due to exfiltration
$\left\{\Delta W_p^{\text{hires,tagged}}\right\}_{\text{OVR}}$	(m)	Subgrid change of tagged ponded water due to overland flow
$\left\{\Delta W_p^{\text{hires,tagged}}\right\}_{\text{SSR}}$	(m)	Subgrid change of tagged ponded water due to exfiltrating subsurface flow
$\left\{\Delta W_p^{\text{tagged}}\right\}_{I}$	(m)]	Change of tagged ponded water due to infiltration excess
E^{tagged}	(m/s)	Tagged surface evaporation
E_d^{tagged}	(m/s)	Tagged direct evaporation
E_t^{tagged}	(m/s)	tagged plant transpiration
$F_{\hat{\theta}}^{\text{tagged}}$	(m/s)	Tagged external forcing in Richard's equation
I^{tagged}	(m/s)	Tagged surface infiltration
$O_{\text{NET}}^{\text{tagged}}$	(m/s)	Net outflow of tagged atmospheric water
P^{source}	(m/s)	Source precipitation
$P_{\text{liq}}^{\text{source}}$	(m/s)	Liquid source precipitation
$P_{\text{solid}}^{\text{source}}$	(m/s)	Solid source precipitation
P^{tagged}	(m/s)	Tagged precipitation at the surface
$P_{\text{bare}}^{\text{tagged}}$	(m/s)	Tagged water falling on bare soil
$q_{\text{sfc}}^{\text{hires,tagged}}$	(m)	Subgrid net tagged surface lateral water flow
$\left\{q_{\text{sfc}}^{\text{hires,tagged}}\right\}^{\text{IN}}$	(m)	Subgrid incoming tagged surface lateral water flow
$\left\{q_{\text{sfc}}^{\text{hires,tagged}}\right\}^{\text{OUT}}$	(m)	Subgrid outgoing tagged surface lateral water flow
$q_{\text{sub}}^{\text{hires,tagged}}$	(m)	Subgrid net tagged subsurface lateral water flow
$\left\{q_{\text{sub}}^{\text{hires,tagged}}\right\}^{\text{IN}}$	(m)	Subgrid incoming tagged subsurface lateral water flow
$\left\{q_{\text{sub}}^{\text{hires,tagged}}\right\}^{\text{OUT}}$	(m)	Subgrid outgoing tagged subsurface lateral water flow
R_G^{tagged}	(m/s)	Tagged underground runoff
R_S^{tagged}	(m/s)	Tagged surface runoff
r_c	(−)	Tagged canopy water ratio
$\left\{r_{\text{Cavail}}^{\text{hires}}\right\}^{\text{local}}$	(−)	Subgrid tagged column-available water ratio at local grid point
$\left\{r_{\text{Cavail}}^{\text{hires}}\right\}^{\text{upstream}}$	(−)	Subgrid tagged column-available water ratio at upstream grid point
$\left\{r_p^{\text{hires}}\right\}^{\text{local}}$	(−)	Subgrid tagged ponded water ratio at local grid point
$\left\{r_p^{\text{hires}}\right\}^{\text{upstream}}$	(−)	Subgrid tagged ponded water ratio at upstream grid point
r_s	(−)	Tagged snow equivalent water content ratio
$r_{\theta_{\text{ice}}}$	(−)	Tagged frozen soil moisture ratio
$r_{\theta_{\text{liq}}}$	(−)	Tagged liquid soil moisture ratio
S^{tagged}	(m)	Tagged terrestrial water storage

θ_{ice}^{tagged}	(−)	Tagged frozen soil moisture
θ_{liq}^{tagged}	(−)	Tagged liquid soil moisture
$\theta_{liq}^{hires,tagged}$	(−)	Subgrid tagged liquid soil moisture
W^{tagged}	(m)	Tagged vertically integrated atmospheric water content
W_c^{tagged}	(m)	Tagged canopy water
W_p^{tagged}	(m)	Tagged ponded water
$W_p^{hires,tagged}$	(m)	Subgrid tagged ponded water
W_s^{tagged}	(m)	Tagged snow equivalent water content at the land surface
W_θ^{tagged}	(m)	Tagged soil moisture content in the soil column
$W_{\theta,0-100}^{tagged}$	(m)	Tagged soil moisture content between 0- and 100-cm depths
$W_{\theta,100-200}^{tagged}$	(m)	Tagged soil moisture content between 100- and 200-cm depths

Mathematical operators

M	Any variable
$(M)_t$	Time derivate operator
$(M)_z$	Terrestrial derivate operator in the vertical direction

Acknowledgments
This research is funded by the German Science Foundation (DFG, SFB/TRR 165). Jianhui Wei is supported financially by the DFG through funding of the AccHydro project (DFG Grant KU 2090/11-1) and Zhenyu Zhang by the Scholarship Council (CSC). This research benefited from scientific collaboration with the DFG Trilateral Project IMAP (Integrating Microwave Link Data for Analysis of Precipitation in Complex Terrain: Theoretical Aspects and Hydrometeorological Applications). ECMWF operational analyses were obtained within the framework of a Special project at the ECMWF. The SVA-TAG procedure was developed at the German Climate Computing Center. The WRF and WRF-Hydro simulations were performed on the computational resource ForHLR II funded by the Ministry of Science, Research and the Arts Baden-Württemberg and DFG ("Deutsche Forschungsgemeinschaft"). We acknowledge the precipitation data set from the ECA&D project (http://www.ecad.eu), the surface evaporation product from the Max Planck Institute for Biogeochemistry (https://climatedataguide.ucar.edu/climate-data/fluxnet-mte-multi-tree-ensemble), and the discharge data set from the Global Runoff Data Center (http://www.bafg.de/GRDC/EN/Home/homepage_node.html). The WRF-Hydro preprocessing tool is available online (https://ral.ucar.edu/projects/wrf_hydro/pre-processing-tools). Special thanks go to Christoph Sörgel, Dominikus Heinzeller, and Hartmut Häfner for the computer support, and three anonymous reviewers for helping to clarify the manuscript.

References

Anyah, R. O., Weaver, C. P., Miguez-Macho, G., Fan, Y., & Robock, A. (2008). Incorporating water table dynamics in climate modeling: 3. Simulated groundwater influence on coupled land–atmosphere variability. *Journal of Geophysical Research*, *113*, D0703. https://doi.org/10.1029/2007JD009087

Arnault, J., Knoche, R., Wei, J., & Kunstmann, H. (2016). Evaporation tagging and atmospheric water budget analysis with WRF: A regional precipitation recycling study for West Africa. *Water Resources Research*, *52*, 1544–1567. https://doi.org/10.1002/2015WR017704

Arnault, J., Rummler, T., Baur, F., Lerch, S., Wagner, S., Fersch, B., et al. (2018). Precipitation sensitivity to the uncertainty of terrestrial water flow in WRF-Hydro: An ensemble analysis for central Europe. *Journal of Hydrometeorology*, *19*(6), 1007–1025. https://doi.org/10.1175/JHM-D-17-0042.1

Arnault, J., Wagner, S., Rummler, T., Fersch, B., Bliefernicht, J., Andresen, S., & Kunstmann, H. (2016). Role of runoff–infiltration partitioning and resolved overland flow on land–atmosphere feedbacks: A case study with the WRF-Hydro coupled modeling system for West Africa. *Journal of Hydrometeorology*, *17*(5), 1489–1516. https://doi.org/10.1175/JHM-D-15-0089.1

Brooks, P. D., Chorover, J., Fan, Y., Godsey, S. E., Maxwell, R. M., McNamara, J. P., & Tague, C. (2015). Hydrological partitioning in the critical zone: Recent advances and opportunities for developing transferable understanding of water cycle dynamics. *Water Resources Research*, *51*, 6973–6987. https://doi.org/10.1002/2015WR017039

Chen, F., & Dudhia, J. (2001). Coupling an advanced land surface–hydrology model with the Penn State–NCAR MM5 modeling system. Part I: Model implementation and sensitivity. *Monthly Weather Review*, *129*(4), 569–585. https://doi.org/10.1175/1520-0493(2001)129<0569:CAALSH>2.0.CO;2

Chen, L., & Dirmeyer, P. A. (2017). Impacts of land-use/land-cover change on afternoon precipitation over North America. *Journal of Climate*, *30*(6), 2121–2140. https://doi.org/10.1175/JCLI-D-16-0589.1

Dieng, D., Smiatek, G., Bliefernicht, J., Heinzeller, D., Sarr, A., Gaye, A. T., & Kunstmann, H. (2017). Evaluation of the COSMO-CLM high-resolution climate simulations over West Africa. *Journal of Geophysical Research: Atmospheres*, *122*, 1437–1455. https://doi.org/10.1002/2016JD025457

Dirmeyer, P. A. (2013). Characteristics of the water cycle and land–atmosphere interactions from a comprehensive reforecast and reanalysis data set: CFSv2. *Climate Dynamics*, *41*(3-4), 1083–1097. https://doi.org/10.1007/s00382-013-1866-x

Dominguez, F., Miguez-Macho, G., & Hu, H. (2016). WRF with water vapor tracers: A study of moisture sources for the North American Monsoon. *Journal of Hydrometeorology*, *17*(7), 1915–1927. https://doi.org/10.1175/JHM-D-15-0221.1

Dudhia, J. (1989). Numerical study of convection observed during the Winter Monsoon Experiment using a mesoscale two-dimensional model. *Journal of the Atmospheric Sciences*, *46*, 3077–3107. https://doi.org/10.1175/1520-0469(1989)046<3077:NSOCOD>2.0.CO;2

Duerinck, H. M., van der Ent, R. J., van de Giesen, N. C., Schoups, G., Babovic, V., & Yeh, P. J. (2016). Observed soil moisture–precipitation feedback in Illinois: A systematic analysis over different scales. *Journal of Hydrometeorology*, *17*(6), 1645–1660. https://doi.org/10.1175/JHM-D-15-0032.1

Ek, M. B., Mitchell, K. E., Lin, Y., Rogers, E., Grummann, P., Koren, V., et al. (2003). Implementation of Noah land surface model advances in the National Centers for Environmental Prediction operational Mesoscale Eta Model. *Journal of Geophysical Research*, *108*(D22), 8851. https://doi.org/10.1029/2002JD003296

Fan, Y., Miguez-Macho, G., Weaver, C. P., Walko, R., & Robock, A. (2007). Incorporating water table dynamics in climate modeling: 1. Water table observation and equilibrium water table simulations. *Journal of Geophysical Research*, *112*, D10125. https://doi.org/10.1029/2006JD008111

Gao, Y., Chen, F., Barlage, M., Liu, W., Cheng, G., Li, X., et al. (2008). Enhancement of land surface information and its impact on atmospheric modeling in the Heihe River Basin, northwest China. *Journal of Geophysical Research*, *113*, D20S90. https://doi.org/10.1029/2008JD010359

Global Runoff Data Center (2015). Twelfth Meeting of the GRDC Steering Committee, 18 –19 June 2015, Koblenz, Germany. - (30 pp). – https://doi.org/10.5675/GRDC_Report_46

Gochis, D. J., Yu, W., & Yates, D. N. (2015). The WRF-Hydro model technical description and user's guide, version 3.0. NCAR Technical Document. 120 pages. Available online at: http://www.ral.ucar.edu/projects/wrf_hydro/

Gupta, H. V., Kling, H., Yilmaz, K. K., & Martinez, G. F. (2009). Decomposition of the mean squared error and NSE performance criteria: Implications for improving hydrological modelling. *Journal of Hydrology*, *377*(1-2), 80–91. https://doi.org/10.1016/j.jhydrol.2009.08.003

Haylock, M. R., Hofstra, N., Klein Tank, A. M. G., Klok, E. J., Jones, P. D., & New, M. (2008). A European daily high-resolution gridded dataset of surface temperature and precipitation. *Journal of Geophysical Research*, *113*, D20119. https://doi.org/10.1029/2008JD10201

Hong, S.-Y., Dudhia, J., & Chen, S.-H. (2004). A revised approach to ice microphysical processes for the bulk parameterization of clouds and precipitation. *MonthlyWeather Review*, *132*, 103–120. https://doi.org/10.1175/1520-0493(2004)132<0103:ARATIM>2.0.CO;2

Hong, S.-Y., & Lim, J.-O. J. (2006). The WRF single-moment 6-class microphysics scheme (WSM6). *J. Korean Meteor. Soc.*, *42*, 129–151.

Hong, S.-Y., Noh, Y., & Dudhia, J. (2006). A new vertical diffusion package with an explicit treatment of entrainment processes. *MonthlyWeather Review*, *134*(9), 2318–2341. https://doi.org/10.1175/MWR3199.1

Hu, H., Dominguez, F., Kumar, P., McDonnell, J., & Gochis, D. (2018). A numerical water tracer model for understanding event scale hydrometeorological phenomena. *Journal of Hydrometeorology*, *19*(6), 947–967. https://doi.org/10.1175/JHM-D-17-0202.1

Im, E., Marcella, M. P., & Eltahir, E. B. (2014). Impact of potential large-scale irrigation on the West African Monsoon and its dependence on location of irrigated area. *Journal of Climate*, *27*(3), 994–1009. https://doi.org/10.1175/JCLI-D-13-00290.1

Insua-Costa, D., & Miguez-Macho, G. (2018). A new moisture tagging capability in the Weather Research and Forecasting model: Formulation, validation and application to the 2014 Great Lake-effect snowstorm. *Earth System Dynamics*, *9*(1), 167–185. https://doi.org/10.5194/esd-9-167-2018

Julien, P. Y., Saghafian, B., & Ogden, F. L. (1995). Raster-based hydrologic modeling of spatially-varied surface runoff. *Water Resources Bulletin*, *31*(3), 523–536. https://doi.org/10.1111/j.1752-1688.1995.tb04039.x

Jung, M., Reichstein, M., & Bondeau, A. (2009). Towards global empirical upscaling of FLUXNET eddy covariance observations: Validation of a model tree ensemble approach using a biosphere model. *Biogeosciences*, *6*(10), 2001–2013. https://doi.org/10.5194/bg-6-2001-2009

Jung, M., Reichstein, M., Ciais, P., Seneviratne, S. I., Sheeld, J., Goulden, M. L., et al. (2010). Recent decline in the global land evapotranspiration trend due to limited moisture supply. *Nature*, *467*(7318), 951–954. https://doi.org/10.1038/nature09396

Karki, R., ul Hasson, S., Gerlitz, L., Schickhoff, U., Scholten, T., & Böhner, J. (2017). Quantifying the added value of convection-permitting climate simulations in complex terrain: a systematic evaluation of WRF over the Himalayas. *Earth System Dynamics*, *8*(3), 507–528. https://doi.org/10.5194/esd-8-507-2017

Kerandi, N., Arnault, J., Laux, P., Wagner, S., Kitheka, J., & Kunstmann, H. (2017). Joint atmospheric-terrestrial water balances for East Africa: A WRF-Hydro case study for the upper Tana River basin. *Theoretical and Applied Climatology*, *131*(3-4), 1337–1355. https://doi.org/10.1007/s00704-017-2050-8

Knoche, H. R., & Kunstmann, H. (2013). Tracking atmospheric water pathways by direct evaporation tagging: A case study for West Africa. *Journal of Geophysical Research: Atmospheres*, *118*, 12,345–12,358. https://doi.org/10.1002/2013JD019976

Larsen, M. A. D., Christensen, J. H., Drews, M., Butts, M. B., & Refsgaard, J. C. (2016). Local control on precipitation in a fully coupled climate-hydrology model. *Scientific Reports*, *6*(1), 22927. https://doi.org/10.1038/srep22927

Laux, P., Nguyen, P. N. B., Cullmann, J., Van, T. P., & Kunstmann, H. (2017). How many RCM ensemble members provide confidence in the impact of land-use land cover change? *International Journal of Climatology*, *37*(4), 2080–2100. https://doi.org/10.1002/joc.4836

Lehner, B., Verdin, K., & Jarvis, A. (2008). New global hydrography derived from spaceborne elevation data. *Eos, Transactions, AGU*, *89*(10), 93–94. https://doi.org/10.1029/2008EO100001

Mahmood, R., Pielke, R. A. Sr., Hubbard, K. G., Niyogi, D., Dirmeyer, P. A., McAlpine, C., et al. (2014). Land cover changes and their biogeophysical effects on climate. *International Journal of Climatology*, *34*(4), 929–953. https://doi.org/10.1002/joc.3736

Maxwell, R. M., Chow, F. K., & Kollet, S. J. (2007). The groundwater-land-surface-atmosphere connection: Soil moisture effects on the atmospheric boundary layer in fully-coupled simulations. *Advances in Water Resources*, *30*, 2447–2466. https://doi.org/10.1016/j.advwatres.2007.05.018

McDonnell, J. J., McGuire, K. J., Aggarwal, P., Beven, K. J., Biondi, D., Destouni, G., et al. (2010). How old is streamwater? Open questions in catchment transit time conceptualization, modelling and analysis. *Hydrological Processes*, *24*(12), 1745–1754. https://doi.org/10.1002/hyp.7796

McGuire, K. J., & McDonnell, J. J. (2006). A review and evaluation of catchment transit time modeling. *Journal of Hydrology*, *330*(3-4), 543–563. https://doi.org/10.1016/j.jhydrol.2006.04.020

Miguez-Macho, G., Fan, Y., Weaver, C. P., Walko, R., & Robock, A. (2007). Incorporating water table dynamics in climate modeling: 2. Formulation, validation, and soil moisture simulation. *Journal of Geophysical Research*, *112*, D13108. https://doi.org/10.1029/2006JD008112

Mlawer, E. J., Taubman, S. J., Brown, P. D., Lacono, M. J., & Clough, S. A. (1997). Radiative transfer for inhomogeneous atmosphere: RRTM, a validated correlated-k model for the long- wave. *Journal of Geophysical Research*, *102*(D14), 16,663–16,682. https://doi.org/10.1029/97JD00237

Niu, G.-Y., Yang, Z.-L., Mitchell, K. E., Chen, F., Ek, M. B., Barlage, M., et al. (2011). The community Noah land surface model with multiparameterization options (Noah-MP): 1. Model description and evaluation with local-scale measurements. *Journal of Geophysical Research*, *116*, D12109. https://doi.org/10.1029/2010JD015139

Pielke, R. A. Sr. (2001). Influence of the spatial distribution of vegetation and soils on the prediction of cumulus Convective rainfall. *Review of Geophysics*, *39*(2), 151–177. https://doi.org/10.1029/1999RG000072

Pielke, R. A. Sr., Pitman, A., Niyogi, D., Mahmood, R., McAlpine, C., Hossain, F., et al. (2011). Land use/land cover changes and climate: Modeling analysis and observational evidence. *WIREs Climate Change*, *2*(6), 828–850. https://doi.org/10.1002/wcc.144

Pleim, J. E. (2007). A combined local and nonlocal closure model for the atmospheric boundary layer. Part I: Model description and testing. *Journal of Applied Meteorology and Climatology*, *46*(9), 1383–1395. https://doi.org/10.1175/JAM2539.1

Quesada, B., Devaraju, N., de Noblet-Ducoudré, N., & Arneth, A. (2017). Reduction of monsoon rainfall in response to past and future land use and land cover changes. *Geophysical Research Letters*, *44*, 1041–1050. https://doi.org/10.1002/2016GL070663

Rahman, M., Sulis, M., & Kollet, S. J. (2015). The subsurface–land surface–atmosphere connection under convective conditions. *Advances in Water Resources*, *83*, 240–249. https://doi.org/10.1016/j.advwatres.2015.06.003

Rummler, T., Arnault, J., Gochis, D., & Kunstmann, H. (2019). Role of lateral terrestrial water flow on the regional water cycle in a complex terrain region: Investigation with a fully coupled model system. *Journal of Geophysical Research: Atmospheres*, accepted, *124*, 507–529. https://doi.org/10.1029/2018JD029004

Senatore, A., Mendicino, G., Gochis, D. J., Yu, W., Yates, D. N., & Kunstmann, H. (2015). Fully coupled atmosphere-hydrology simulations for the central Mediterranean: Impact of enhanced hydrological parameterization for short and long time scales. *Journal of Advances in Modeling Earth Systems*, *7*, 1693–1715. https://doi.org/10.1002/2015MS000510

Seneviratne, S. I., Corti, T., Davin, E. L., Hirschi, M., Jaeger, E. B., Lehner, I., et al. (2010). Investigating soil moisture–climate interactions in a changing climate: A review. *Earth Science Review*, *99*(3-4), 125–161. https://doi.org/10.1016/j.earscirev.2010.02.004

Serdeczny, O., Adams, S., Baarsch, F., Coumou, D., Robinson, A., Hare, W., et al. (2016). Climate change impacts in Sub-Saharan Africa: from physical changes to their social repercussions. *Regional Environmental Change*, *17*(6), 1585–1600. https://doi.org/10.1007/s10113-015-0910-2

Skamarock, W. C., & Klemp, J. B. (2008). A time-split nonhydrostatic atmospheric model for weather research and forecasting applications. *Journal of Computational Physics*, *227*, 3465–3485. https://doi.org/10.1016/j.jcp.2007.01.037

Smiatek, G., Kunstmann, H., & Senatore, A. (2016). EURO-CORDEX regional climate model analysis for the Greater Alpine Region: Performance and expected future change. *Journal of Geophysical Research: Atmospheres*, *121*, 7710–7728. https://doi.org/10.1002/2015JD024727

Sodemann, H., Wernli, H., & Schwierz, C. (2009). Sources of water vapour contributing to the Elbe flood in August 2002—A tagging study in a mesoscale model. *Quarterly Journal of the Royal Meteorological Society*, *135*(638), 205–223. https://doi.org/10.1002/qj.374

Sprenger, M., Seeger, S., Blume, T., & Weiler, M. (2016). Travel times in the vadose zone: Variability in space and time. *Water Resources Research*, *52*, 5727–5754. https://doi.org/10.1002/2015WR018077

Strahler, A. N. (1957). Quantitative analysis of watershed geomorphology. *Transactions of the American Geophysical Union*, *38*(6), 913–920. https://doi.org/10.1029/tr038i006p00913

Van der Ent, R. J., & Savenije, H. H. G. (2011). Length and time scales of atmospheric moisture recycling. *Atmospheric Chemistry and Physics*, *11*(5), 1853–1863. https://doi.org/10.5194/acp-11-1853-2011

Wagner, S., Fersch, B., Yuan, F., Yu, Z., & Kunstmann, H. (2016). Fully coupled atmospheric-hydrological modeling at regional and long-term scales: Development, application, and analysis of WRF-HMS. *Water Resources Research*, *52*, 3187–3211. https://doi.org/10.1002/2015WR018185

Wei, J., Knoche, H. R., & Kunstmann, H. (2015). Contribution of transpiration and evaporation to precipitation: An ET-Tagging study for the Poyang Lake region in Southeast China. *Journal of Geophysical Research: Atmospheres*, *120*, 6845–6864. https://doi.org/10.1002/2014JD022975

Wei, J., Knoche, H. R., & Kunstmann, H. (2016). Atmospheric residence times from transpiration and evaporation to precipitation: An age-weighted regional evaporation tagging approach. *Journal of Geophysical Research: Atmospheres*, *121*, 6841–6862. https://doi.org/10.1002/2015JD024650

Zhang, Z., Arnault, J., Wagner, S., Laux, P., & Kunstmann, H. (2019). Impact of lateral terrestrial water flow on land-atmosphere interactions in the Heihe river basin in China: Fully coupled modeling and precipitationrecycling analysis. *Journal of Geophysical Research: Atmospheres*. https://doi.org/10.1029/2018JD030174